1-22-2016

Identification of Critical Paraoxonase 1 Residues Involved in High Density Lipoprotein Interaction

Xiaodong Gu
Cleveland Clinic

Ying Huang
Cleveland State University

Bruce S. Levison
Cleveland Clinic

Gary Gerstenecker
Cleveland State University

Anthony J. DiDonato
Cleveland Clinic

See next page for additional authors

Recommended Citation

Gu, Xiaodong; Huang, Ying; Levison, Bruce S.; Gerstenecker, Gary; DiDonato, Anthony J.; Hazen, Leah B.; Lee, Joonsue; Gogonea, Valentin; DiDonato, Joseph A.; and Hazen, Stanley L., "Identification of Critical Paraoxonase 1 Residues Involved in High Density Lipoprotein Interaction" (2016). *Chemistry Faculty Publications*. 315.
https://engagedscholarship.csuohio.edu/scichem_facpub/315

THE JOURNAL OF BIOLOGICAL CHEMISTRY VOL. 291, NO. 4, pp. 1890–1904, January 22, 2016

Identification of Critical Paraoxonase 1 Residues Involved in High Density Lipoprotein Interaction*

Received for publication, July 11, 2015, and in revised form, November 12, 2015 Published, JBC Papers in Press, November 13, 2015, DOI 10.1074/jbc.M115.678334

Xiaodong Gu[‡1], Ying Huang[‡], Bruce S. Levison[‡], Gary Gerstenecker[§], Anthony J. DiDonato[‡], Leah B. Hazen[‡], Joonsue Lee[‡], Valentin Gogonea[‡§], Joseph A. DiDonato[‡], and Stanley L. Hazen[‡¶2]

From the [‡]Department of Cellular and Molecular Medicine, Center for Cardiovascular Diagnostics and Prevention, and [¶]Department of Cardiovascular Medicine, Cleveland Clinic, Cleveland, Ohio 44195 and the [§]Department of Chemistry, Cleveland State University, Cleveland, Ohio 44115

Paraoxonase 1 (PON1) is a high density lipoprotein (HDL)-associated protein with atherosclerosis-protective and systemic anti-oxidant functions. We recently showed that PON1, myeloperoxidase, and HDL bind to one another *in vivo* forming a functional ternary complex (Huang, Y., Wu, Z., Riwanto, M., Gao, S., Levison, B. S., Gu, X., Fu, X., Wagner, M. A., Besler, C., Gerstenecker, G., Zhang, R., Li, X. M., Didonato, A. J., Gogonea, V., Tang, W. H., *et al.* (2013) *J. Clin. Invest.* 123, 3815–3828). However, specific residues on PON1 involved in the HDL-PON1 interaction remain unclear. Unambiguous identification of protein residues involved in docking interactions to lipid surfaces poses considerable methodological challenges. Here we describe a new strategy that uses a novel synthetic photoactivatable and click chemistry-taggable phospholipid probe, which, when incorporated into HDL, was used to identify amino acid residues on PON1 that directly interact with the lipoprotein phospholipid surface. Several specific PON1 residues (Leu-9, Tyr-185, and Tyr-293) were identified through covalent cross-links with the lipid probes using affinity isolation coupled to liquid chromatography with on-line tandem mass spectrometry. Based upon the crystal structure for PON1, the identified residues are all localized in relatively close proximity on the surface of PON1, defining a domain that binds to the HDL lipid surface. Site-specific mutagenesis of the identified PON1 residues (Leu-9, Tyr-185, and Tyr-293), coupled with functional studies, reveals their importance in PON1 binding to HDL and both PON1 catalytic activity and stability. Specifically, the residues identified on PON1 provide important structural insights into the PON1-HDL interaction. More generally, the new photoactivatable and affinity-tagged lipid probe developed herein should prove to be a valuable tool for identifying contact sites supporting protein interactions with lipid interfaces such as found on cell membranes or lipoproteins.

Ever since the Framingham heart study revealed the inverse relationship between high density lipoprotein (HDL) cholesterol levels and the risk of coronary artery disease, the structure and biological functions of HDL have been under intense scrutiny (1–6). HDL and its major structural protein component, apolipoprotein A-I (apoA-I), play a pivotal role in mediating reverse cholesterol transport, which describes the process of cholesterol removal from peripheral tissues for ultimate elimination from the body by excretion (2, 7–9). Although facilitation of reverse cholesterol transport through cholesterol acceptor activity is considered a major function of HDL particles, ample evidence shows additional functions exist, such as anti-oxidant, anti-inflammatory, and anti-tumorigenic activities, and the shuttling of microRNAs or lipid-signaling molecules (10–16). HDL is a highly heterogeneous array of distinct particles, with differing associated proteome and peptidome (17–22). In addition to exchangeable apolipoproteins, early proteomics studies revealed the HDL-associated proteome includes known participants critical to hemostasis and thrombosis, innate and adaptive immune function, growth factors and various receptors, and hormone-associated proteins (17, 20). In the years that have followed since the original HDL proteomics studies, subsequent reports have confirmed and expanded upon these earlier findings, revealing a remarkably complex HDL-associated proteome that can differ as a function of disease status or susceptibility (23–25). Thus, alterations in HDL function appear to be, at least in part, dictated by changes in the complement of HDL-associated proteins present, with distinct HDL particle subpopulations composed of unique and dynamically changing clusters of specific HDL-associated proteins (24–29).

One subpopulation of HDL particles of interest are those enriched in paraoxonase 1 (PON1). Early genetic and dietary studies in mouse models revealed PON1 to be an atheroprotective protein (30). Localized to the HDL particle, PON1 has been shown to contribute to HDL-associated anti-oxidative, anti-inflammatory, and cholesterol efflux functions (10, 12, 24, 31). PON1 has also been shown to stimulate HDL-dependent nitric

* This work was supported in part by National Institutes of Health Grants P01 HL076491 and P01 HL103453. S. L. H. is named as co-inventor on pending and issued patents held by the Cleveland Clinic relating to cardiovascular diagnostics and therapeutics. S. L. H. reports having been paid as a consultant for the following companies: Esperion and Procter & Gamble. S. L. H. reports receiving research funds from Abbott, Astra Zeneca, Liposcience Inc., Procter & Gamble, Pfizer Inc., Roche Diagnostics, and Takeda. S. L. H. reports having the right to receive royalty payments for inventions or discoveries related to cardiovascular diagnostics or therapeutics from the following companies: Cleveland HeartLab, Siemens, Esperion, Frantz Biomarkers, LLC. The content is solely the responsibility of the authors and does not necessarily represent the official views of the National Institutes of Health.

[1] Supported in part by a Fellowship Award from the American Heart Association.

[2] Supported in part by a gift from the Leonard Krieger endowment. To whom correspondence should be addressed: Dept. of Cellular and Molecular Medicine, Lerner Research Institute, Cleveland Clinic, 9500 Euclid Ave., NC-10, Cleveland, OH 44195. Tel.: 216-4459763; Fax: 216-444-9404; E-mail: hazens@ccf.org.

oxide (NO) production by endothelial nitric-oxide synthase (10, 32–34). PON1 possesses both esterase and lactonase catalytic activities *in vitro* but has unclear substrate(s) *in vivo* (35). A role for PON1 protection from atherosclerosis *in vivo* has been supported by studies showing PON1 knock-out mice have accelerated atherosclerosis (36), and human PON1 transgenic mice demonstrate both protection from atherosclerosis and reduced indices of systemic oxidative stress (31, 37). In human studies, a striking correlation between multiple systemic measures of oxidant stress and serum PON1 activity measures has also been established (12, 31). Moreover, reduced systemic PON1 activity has been shown to predict increased prospective risks for major adverse cardiac events in multiple distinct clinical cohorts (12, 38–41). Thus, there is considerable *in vitro* and *in vivo* evidence to support PON1 as an important mediator of many anti-inflammatory, anti-oxidant, and atheroprotective activities of HDL.

Knowledge at the structural level of how HDL-associated proteins interact with HDL particles is in its infancy. In prior studies, we showed that HDL forms a functional ternary complex with PON1 and myeloperoxidase (31), an oxidant-generating enzyme linked to development of atherosclerosis (42–48). Each member of the ternary complex was shown to impact the function of the other *in vivo* (31). Residues involved in the protein-protein interaction between PON1 and apoA-I of HDL, or between myeloperoxidase and apoA-I of HDL, have thus far been delineated using hydrogen deuterium exchange mass spectrometry-based methodology as a discovery platform, coupled with site-specific mutagenesis and functional studies to determine the significance of the residues involved (31, 49). Despite the many recent advances made, a full understanding of how PON1 interacts with HDL remains unclear. For example, PON1 binding to HDL lipid and membrane surfaces is known to be essential for its stability and catalytic activity (31); however, the interaction sites between PON1 and the lipid interface of HDL remain unknown. Indeed, tools for defining contact residues between proteins and phospholipid surfaces such as on a membrane bilayer, or a lipoprotein particle, are not readily available.

Herein, we describe development, characterization, and application of a novel tool to interrogate contact residues that support tight binding interactions with phospholipid surfaces, a synthetic photoactivatable and "clickable" phosphatidylcholine analogue (pac-PC).[3] Using PON1-HDL interactions as a test case, we illustrate the facile use of this new technology, defining several key residues on PON1 essential for PON1 docking to HDL, PON1 catalytic activity, and stability. The use of pac-PC incorporated into recombinant HDL particles or membrane bilayers may thus serve as a universal strategy to facilitate identification of residues critical for protein docking with the lipid surface of lipoproteins or cell membranes.

[3] The abbreviations used are: pac-PC, photoactivatable and clickable-phosphatidylcholine; rHDL, reconstituted nascent HDL; Ni-NTA, nickel-nitrilotriacetic acid; DMPA, 1,2-dimyristoyl-*sn*-glycero-3-phosphate; SPR, surface plasmon resonance.

Experimental Procedures

General Methods—All solvents used for synthesis were distilled under a nitrogen atmosphere prior to use, and all materials were obtained from Sigma unless specified otherwise. Chromatography was performed with ACS-grade solvents. Progress of synthetic reactions was monitored by thin layer chromatography, and R_f values are quoted for silica gel-coated plates of 0.25-mm layer thickness. The plates were visualized with iodine. Flash column chromatography (50) was performed on 230–400-mesh silica gel supplied by EMD Millipore. Protein content was measured using the Markwell-modified Lowry method (51) with bovine serum albumin as a standard. PON1 activity measurements (paraoxonase and arylesterase activities) were performed as described previously (39). Proton magnetic resonance (^{1}H NMR) spectra were recorded on a Varian Inova AS400 spectrometer operating at 600 MHz. Proton chemical shifts are reported as parts per million (ppm) on the δ scale relative to $CDCl_3$ (δ 7.24). ^{1}H NMR spectral data are tabulated in terms of multiplicity of proton absorption (s, singlet; d, doublet; t, triplet; m, multiplet; br, broad), coupling constants (Hz), and number of protons. The UV light source (365 nm) was supplied by a Spectroline Model ENF-280C lamp suspended just over the top of the sample tubes.

Chemical Syntheses of 1,2-Dimyristoyl-sn-glycero-3-phospho-2-(3-methyl-3H-diazirin-3-yl)ethanol—1,2-Dimyristoyl-*sn*-glycero-3-phosphate (DMPA, 200 mg, 0.33 mmol, Corden-Pharma, Boulder, CO), 2-(3-methyl-3*H*-diazirin-3-yl)ethanol (70 μl, 0.7 mmol) (52, 53), and 2,4,6-triisopropylbenzenesulfonyl chloride (300 mg, 0.96 mmol) were dissolved in 10 ml of anhydrous pyridine, and the reaction mixture was stirred overnight at room temperature. The reaction was quenched by adding 0.5 ml of water. Pyridine was removed by rotary evaporation. The residue was suspended in 70 ml of cold ether at 4 °C overnight. After filtration, the ether was removed by rotary evaporation. The crude product was purified by silica gel chromatography eluting with 10% methanol in chloroform to obtain the pure product (139.4 mg, yield 63%, R_f= 0.37 ($CHCl_3$/CH_3OH/H_2O = 15:5:0.5)). ^{1}H NMR (600 MHz, $CDCl_3$) δ 5.28 (br, 1H), 4.42 (br, 1H), 4.18 (br, 1H), 3.98 (br, 2H), 3.77 (br, 2H), 2.40–2.20 (4H), 1.70–1.50 (6H), 1.30–1.10 (40H), 1.03 (s, 3H), 0.85 (t, 6H). Negative ESI-MS/MS analysis yielded the following diagnostic parent and fragment ions: *m*/*z* 673.8 $[M - H]^-$; *m*/*z* 645.6, 435.5, 227.6.

Chemical Syntheses of 1-Myristoyl-sn-glycero-3-phospho-2-(3-methyl-3H-diazirin-3-yl)ethanol—1,2-Dimyristoyl-*sn*-glycero-3-phosphatidyl-2-(3-methyl-3*H*-diazirin-3-yl)ethanol (100 mg, 0.15 mmol) in a 50-ml centrifuge tube as dry film was suspended in 20 ml of PBS buffer (10 mM, pH 8.0, and containing $CaCl_2$ 5 mM) and was vortexed for 5 min. 500 μl of phospholipase A_2 (100 units, Sigma P6534-10MG) was added. The resulting mixture was gently vortexed for another 2 min and incubated at 37 °C in a shaker overnight. Lipids were extracted by the Bligh and Dyer method (54), and the aqueous phase was extracted with chloroform (10 ml 2 times). Organic solvents were combined and evaporated. The crude product was purified on a silica gel column eluting with 15% methanol in chloroform to obtain the pure product (45 mg, yield 65%, R_f = 0.2,

25% methanol in chloroform). Negative ESI-MS/MS analysis yielded the following parent and diagnostic fragment ions: *m*/*z* 463.7 $[M - H]^-$; *m*/*z* 435.6, 365.5, 227.7.

Chemical Syntheses of 1-Myristoyl-2-(10-undecynoyl)-sn-glycero-3-phospho-2-(3-methyl-3H-diazirin-3-yl)ethanol (pac-PC)—1-Myristoyl-*sn*-glycero-3-phosphatidyl-2-(3-methyl-3*H*-diazirin-3-yl)ethanol (20 mg, 0.043 mmol), 10-undecynoic acid (40 mg, 0.22 mmol), *N,N′*-dicyclohexylcarbodiimide (26 mg, 0.126 mmol), and 4-dimethylaminopyridine (5 mg, 0.043 mmol) were dissolved in 2 ml of anhydrous chloroform and stirred at room temperature for 48 h. Solvents were removed by rotary evaporation. The crude product was purified on a silica gel column eluted with 10% methanol in chloroform to deliver the final product (20.4 mg, yield 75%, $R_f = 0.36$ with 20% methanol in chloroform). ^{1}H NMR (600 MHz, $CDCl_3$) δ 5.28 (br, 1H), 4.35 (br, 2H), 4.14 (br, 2H), 4.02 (br, 1H), 3.82 (br, 1H), 2.40–2.20 (4H), 2.20–2.10 (2H), 1.92 (m, 1H), 1.70–1.55 (6H), 1.50 (m, 2H), 1.30–1.10 (28H), 1.04 (s, 3H), 0.86 (t, 3H). Negative ESI-MS/MS analysis yielded the following diagnostic parent and fragment ions: *m*/*z* 627.7 $[M - H]^-$; *m*/*z* 599.5, 435.5, 228.3, 182.1.

Preparation of Reconstituted Nascent HDL Containing pac-PC—All human biological materials were obtained from participants that gave written informed consent for protocols approved by the Cleveland Clinic Institutional Review Board. Human HDL was isolated from plasma of healthy volunteers by sequential buoyant density ultracentrifugation using KBr to adjust density to the range of 1.07–1.21 g/ml, as described previously (55–57). Lipid-free human apoA-I was prepared by delipidation of isolated human HDL using methanol/ether/chloroform followed by ion exchange chromatography. The purity of isolated human apoA-I was verified by SDS-PAGE. Reconstituted nascent HDL (rHDL) was prepared using the sodium cholate dialysis method of Matz and Jonas (58) as modified by Barter and co-workers (59). An initial molar ratio of 98:2:10:1 of 1-palmitoyl-2-oleoyl-*sn*-glycero-3-phosphocholine/pac-PC/cholesterol/isolated human apoA-I was used for reconstituted HDL preparation.

Photoactivatable Cross-linking between pac-PC and Human apoA-I or PON1—Control studies showed that pac-PC is stable (at least on the time scale of many minutes to hour) under normal ambient light conditions. All studies described were performed under ambient light conditions. Nonetheless, exposure of pac-PC to light was minimized at all times (except for UV exposure), by keeping the photo-lipid in screw cap glass reaction vials wrapped in foil.

(i) The cross-linking between pac-PC and human apoA-I/rHDL with pac-PC (human apoA-I concentration of 70 μM) in 0.5 ml of 50 mM PBS buffer at pH 7.0 was transferred into small glass vials on ice and then directly exposed to 365 nm UV light for 1 min. Proteins were then precipitated by adding 9 ml of methanol/chloroform/ether, 1:1:2.5 (v/v/v).

(ii) The cross-linking between pac-PC and PON1/rHDL with pac-PC (human apoA-I concentration of 70 μM) in 0.5 ml of 50 mM PBS buffer at pH 7.0 was incubated with recombinant His-tagged PON1 (rPON1, 30 μM, in 0.5 ml of 50 mM Tris buffer with 1 mM $CaCl_2$, pH 7.0) that was expressed and purified from *Escherichia coli,* as described previously (60). The mixture was incubated at 37 °C for 1 h. This mixture was then transferred into small glass vials on ice and directly exposed to a 365-nm UV light for 1 min. Proteins were then precipitated by adding 18 ml of methanol/chloroform/ether, 1:1:2.5 (v/v/v). The precipitated proteins (mixture of apoA-I and PON1) were dissolved in 1 ml of PBS buffer (50 mM, pH 7.0) with 1% SDS and diluted by addition of 4 ml of PBS buffer (to reduce SDS concentration to 0.2%). Nickel-nitrilotriacetic acid resin (Ni-NTA, 500 μl, pre-washed and equilibrated in PBS buffer, 50 mM, pH 7.0) was added to enrich His-tagged PON1 and to remove human apoA-I. rPON1 was eluted with PBS buffer (50 mM, pH 7.0) containing 0.2% SDS and 200 mM imidazole. rPON1 was again precipitated by using methanol/chloroform/ether, 1:1:2.5 (v/v/v).

Adding Biotin Tag to pac-PC Cross-linked Proteins through Click Chemistry—Precipitated protein (apoA-I or rPON1) that had been cross-linked with the pac-PC was dissolved in 1 ml of PBS buffer (50 mM, pH 7.0, and with 1% SDS). Biotin-azide (61) (4 μl, 30 mM in dimethylformamide) was added, and the mixture was vortexed for 1 min. Then, freshly made tris(2-carboxyethyl)phosphine (20 μl, 50 mM in water) was added, followed by the addition of tris[(1-benzyl-1*H*-1,2,3-triazol-4-yl)methyl] amine (20 μl, 5 mM in DMSO/*t*-butanol = 1:4), and the mixture was vortexed for another 1 min. The reaction was initiated with $CuSO_4$ (50 μl, 20 mM stock solution in water) and the mixture was vortexed for 1 min. The reaction mixture was left at room temperature for 1 h (and vortexed after 30 min). Reaction product was transferred into Slide-a-Lyzer dialysis cassettes (Thermo Scientific) and dialyzed against 4 liters of PBS buffer at 4 °C (buffer changed three times in 24 h).

Affinity Purification of pac-PC-modified Peptides—The affinity purification of pac-PC cross-linked proteins and subsequent on-bead trypsin/chymotrypsin digestion steps were performed using the general tandem orthogonal proteolysis strategy described by Weerapana *et al.* (62). Briefly, photoactivatable lipid probe (pac-PC) cross-linked and biotin-tagged proteins (apoA-I or rPON1) were incubated with neutravidin beads (200 μl, 1:1 slurry, pre-washed and equilibrated in PBS buffer) for 3 h at room temperature. Supernatant was removed by centrifugation at 1400 × *g* for 3 min. Neutravidin beads were washed by 5 ml of PBS (with 0.2% SDS) three times and followed by 5 ml of water. Beads were transferred into a low retention Eppendorf tube and incubated with a premixed solution (200 μl of 1 M urea/PBS, 2 μl of 1 M calcium chloride in water, and 4 μl of 0.5 μg/μl trypsin or chymotrypsin) at 37 °C overnight with rotations. Neutravidin beads were washed with PBS buffer (3 × 500 μl) and water (3 × 500 μl). To release the biotinylated peptides from neutravidin beads, the beads were treated with 50:50 (v/v) water/acetonitrile containing 0.1% trifluoroacetic acid (200 μl, 65 °C, 5 min) as described previously (63). Beads were removed via filtration through a spin column and washed with 50:50 (v/v) water/acetonitrile (2 × 100 μl) for a total elution volume of 400 μl. The solvent was evaporated under N_2 flow to a final volume of ~25 μl and was diluted by another 25 μl of 0.1% formic acid/water. For the base treatment, sodium hydroxide (1 M in water, 5 μl) was added, and the resulting mixture was incubated at room temperature for 3 h. Then acetic acid (2 M in water, 3 μl) was added to neutralize the sample. The samples

were analyzed by liquid chromatography with on-line electrospray ionization tandem mass spectrometry (LC/MS/MS).

Mass Spectrometry Analysis—All mass spectrometry analyses were performed under the Xcalibur data system using Proxeon Easy-nLC coupled to a LTQ Orbitrap Velos mass spectrometer (Thermo Scientific) with a nano-LC electrospray ionization source. Samples were first pressure-loaded onto an IntegraFrit sample trap (inner diameter 100 μm, length 2.5 cm, New Objective) and separated by a PicoFrit column (stock number PF360-75-15-N-5, New Objective) packed in our laboratory (packing material: C18, 300 Å, 5 μm from Cobert Associates). Mobile phase was as follows: buffer A/water with 0.1% formic acid; buffer B/acetonitrile with 0.1% formic acid. The HPLC gradient started with 5% B and increased to 40% B over 60 min, then increased to 80% B over 5 min, and held at 80% B for another 10 min. For repeat injections on autosampler, the column was re-equilibrated for the next sample by decreasing to 5% B over 2 min and held at this solvent composition for 20 min. Flow rate was 0.2 μl/min. The applied spray voltage of the nano-LC electrospray ionization source was 2.0 kV. For MS_2 data collection, one full scan by Orbitrap was followed by 10 data-dependent scans of the most intense ions by ion trap. Dynamic exclusion was also applied so that any ions that had been repeatedly scanned three times in 60 s would be excluded for scan for 3 min.

Mass spectra were subject to SEQUEST (64) (Thermo Scientific) and searched against a PON1.fasta database. A static modification +926.532, corresponding to the lipid probe, was applied to each amino acid residue. SEQUEST output files were filtered by XCorr (cross-correlation value, minimal XCorr = 1.8(+1), 2.5(+2), 3.5(+3) as described in the DTASelect (65)). For base-treated samples, a static modification of +226.061 corresponding to a glycerol phosphate group was used. Other possible modifications were also applied during the SEQUEST search, including oxidation on methionine (+16), deamination of glutamine and asparagine (+1), and dehydration of serine and threonine (−18). All targeted peptides spectra were examined by manual inspection.

Site-specific Mutations of Recombinant Paraoxonase 1 (rPON1)—Site-specific mutants of rPON1 used included the G3C9 PON1 clone (60) on the wild type (WT) backbone sequence. The pan-E PON1 mutant (L9E, Y185E, and Y29E), pan-K PON1 mutant (L9K, Y185K, and Y293K), PON1 (Y293K), and PON1 (Y294K) with a His_8 tag directly at their C terminus were prepared from codon-optimized WT rPON1 directly synthesized by GenScript (Piscataway, NJ) and cloned at NcoI-HindIII restriction sites into the pBAD vector (Invitrogen). Competent TOP10 (Invitrogen) *E. coli* cells were transfected with the plasmids for the expression of the recombinant proteins. Wild type and mutant rPON1s were purified by Ni-NTA affinity chromatography to homogeneity, with purity of proteins confirmed by SDS-PAGE.

Spectral Studies of rPON1 Mutants—Far-UV circular dichroism spectra were recorded on a Pistar180 spectropolarimeter (Applied Photophysics, Surrey, UK). Standardization was performed with an aqueous solution of 0.06% ammonium *d*-(+)-10-camphor sulfonate at a wavelengths of 260 to 200 nm and with a path length of 10 mm. rPON1 forms (WT, pan-E, and pan-K mutants) were prepared as 0.1 mg/ml samples in 10 mM phosphate buffer, pH 7.0, supplemented with 0.2 mM $CaCl_2$, and analyzed at ambient temperature in continuous scan mode with a 1-nm bandwidth (100,000 counts/step).

Surface Plasmon Resonance (SPR)—Full time course kinetic determinations of k_{on}, k_{off}, and apparent equilibrium dissociation constants K_d for rHDL interaction with rPON1 forms were determined using SPR using a BIAcore 3000 SPR biosensor (BIAcore, AB). Briefly, rHDL was directly immobilized on a CM5 sensor chip. To determine the K_d value between distinct rPON1 and rHDL, rPON1 ranging from 500 to 2000 nM were prepared in PON1 activity buffer (50 mM Tris, 50 mM NaCl, 1 mM $CaCl_2$, pH 8.0) and flowed over the surface of the sensor chip at a rate of 20 μl/min. At the end of each cycle, surfaces of the sensor chips were regenerated by injection of 15 mM HCl at the same flow rate. Apparent K_d values were obtained by fitting background-subtracted SPR binding data to the 1:1 binding with drifting baseline model within the BIAevaluation software version 4.0.

Stability Studies of rPON1 Mutants—rPON1 was preincubated with rHDLs (2 eq) or 0.1% tergitol (NP-10, Sigma) in PON1 activity buffer (50 mM Tris, 50 mM NaCl, and 1 mM $CaCl_2$, pH 8.0) at 37 °C for 30 min. Inactivation was initiated by adding an equal volume of inactivation buffer (10 mM EDTA and 20 mM β-mercaptoethanol in 50 mM Tris, pH 8.0) and incubating the samples at 37 °C. Aliquots were taken at various time points, and the arylesterase activity was examined as described previously (39).

Results

Photoactivatable Lipid Probe Design and Chemical Synthesis—Plasma HDL particles represent an ensemble of lipidated apoA-I core lipoprotein (75% protein mass of HDL) with numerous distinct interacting HDL-associated proteins. Remarkably, despite the interest in HDL biology and the role in cardiovascular disease, an understanding of the structural regions on virtually all HDL-associated proteins critical for docking to the lipoprotein lipid surface is poorly defined. This is because few specific and effective tools exist for direct detection of protein contact points with lipid surfaces, whether it be a lipoprotein, a cell membrane, or a microparticle. To address this unmet need, we designed a photoactivatable and clickable phospholipid probe, pac-PC (Fig. 1*A*). Phosphatidylcholine is the most abundant class of phospholipid in most lipoproteins and membranes. Our photoaffinity lipid (pac-PC) is an analogue of phosphatidylcholine, which harbors a diazirine ring that replaced the trimethylamine moiety of the choline polar headgroup. Upon exposure to ultraviolet (UV, 365 nm) radiation, the diazirine ring readily expels N_2 generating a reactive diradical carbene species. Carbenes rapidly insert into proximate protein backbones or side chains in nanoseconds, and if not are then scavenged by water at near the diffusion-limited rate. Thus, our probe design ensures that detection of a covalent adduct between the phospholipid probe and a protein indicates the existence of a tight enough binding interaction to exclude water (66). In addition, to facilitate subsequent affinity isolation of adducts, we also introduced a terminal alkyne group on an *sn*-2 position aliphatic chain, providing a useful handle

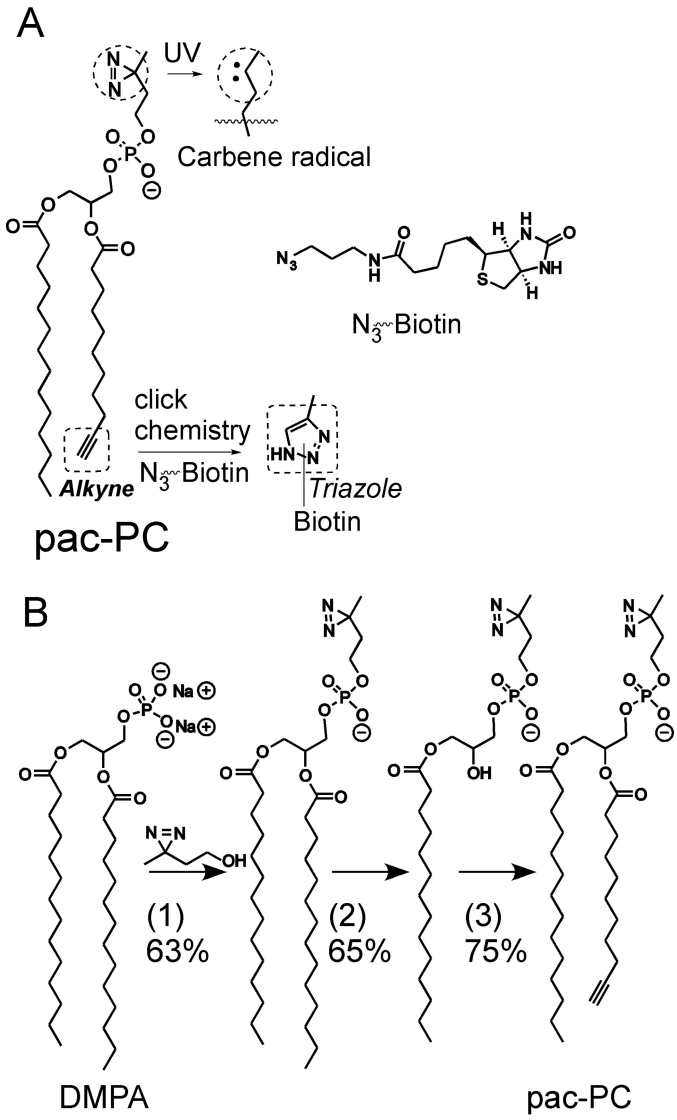

FIGURE 1. **Design and chemical synthesis of the lipid probe pac-PC.** *A,* chemical structure of pac-PC. pac-PC is an analogue of phosphatidylcholine, with two extra function groups as follows: one diazirine group (in *dashed circle*) on *sn*-3 headgroup and one alkyne group (in *dashed square*) on *sn*-2 fatty acid side chain terminal. The carbene di-radical (in *dashed circle*) is generated after UV irradiation. The terminal alkyne reacts with biotin azide to give a triazole (in *dashed square*). *B,* chemical synthesis of pac-PC began from a commercially available lipid (*DMPA*). Briefly, after being coupled with 2-(3-methyl-3*H*-diazirin-3-yl)ethanol, the *sn*-2 side chain was removed through phospholipase A_2-catalyzed hydrolysis. Further reaction of the lyso-lipid with 10-undecynoic acid in the presence of coupling reagents dicyclohexylcarbodiimide (*DCC*) and 4-dimethylaminopyridine (*DMAP*) delivered the final product, pac-PC. Details are under "Experimental Procedures."

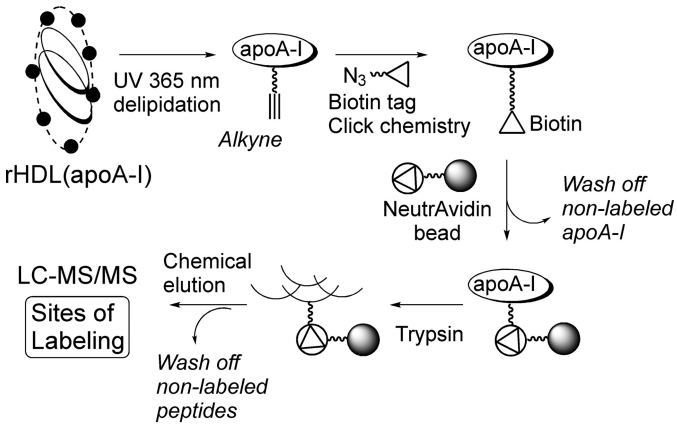

FIGURE 2. **Experimental scheme using pac-PC to investigate pac-PC-apoA-I interaction.** rHDL was prepared as described under "Experimental Procedures" and contained 2 mol % of pac-PC. After UV irradiation, the pac-PC/apoA-I cross-linking products were biotinylated using click chemistry. Biotin-tagged pac-PC/apoA-I adducts were enriched by neutravidin collection and trypsinized, and unbound peptides were washed away. Following the wash step, pac-PC-modified apoA-I peptides were eluted from the beads. In later experiments, base hydrolysis of pac-PC-modified peptides was incorporated at this step to remove the bulk of the lipid side chains allowing accurate software interrogation of modified peptide adducts by analysis using LC/MS/MS. Details are under "Experimental Procedures."

for the later addition of a biotin tag through highly efficient and selective click chemistry (Fig. 1*A*) (67, 68).

The synthetic route to the new lipid probe, pac-PC, is shown in Fig. 1*B*. The chemical synthesis is described in detail under "Experimental Procedures" and began from a commercially available lipid (DMPA). Briefly, after being coupled with 2-(3-methyl-3*H*-diazirin-3-yl)ethanol (69), the *sn*-2 side chain was removed through phospholipase A_2-catalyzed hydrolysis (70). Further reaction of the lysolipid with 10-undecynoic acid in the presence of coupling reagents dicyclohexylcarbodiimide and 4-dimethylaminopyridine delivered the final product, pac-PC (71). The synthesized lipid probe was purified by HPLC and extensively characterized by nuclear magnetic resonance (NMR) and mass spectrometry to confirm its purity and validate its structure, as outlined under "Experimental Procedures."

Photoactivatable Lipid (pac-PC) Cross-linked with ApoA-I in HDL—Photoactivatable lipids have been used to isolate and identify proteins that interact with lipids (72). However, subsequent mass spectrometry analyses to define the exact contact residues of target proteins remain a daunting challenge, as the methods to selectively identify precisely the amino acid residues has not yet been developed. Because apoA-I interacts with phospholipids in nascent HDL particles, we initially examined the interaction of pac-PC with apoA-I in HDL to develop the necessary analytical and mass spectrometry methods. The experimental scheme we used to study lipid-protein interaction in nascent HDL is outlined in Fig. 2. rHDL was prepared as outlined under "Experimental Procedures" using a modified sodium cholate dialysis method containing a low mol % of the photoactivatable lipid probe, pac-PC, to minimize potential structural perturbations to the particle. Control studies (equilibrium native PAGE and dual beam light scattering) showed that the rHDL particles thus generated had similar size compared with rHDL lacking the probe (data not shown). Following exposure to UV irradiation, the pac-PC adduct was biotinylated using click chemistry as outlined under "Experimental Procedures." Tagged apoA-I was then subject to neutravidin affinity column enrichment followed by on-bead trypsin digestion, as described under "Experimental Procedures." Following a wash step, pac-PC-modified apoA-I peptides were eluted from the beads and then analyzed by LC/MS/MS (Fig. 2).

Despite initial efforts to deconvolute the raw spectra with SEQUEST searches, no modified peptides were identified (even when the XCorr values were lowered to 1.0(1+), 2.0(2+), 3.0(3+)). However, manual inspection of the raw peptide spec-

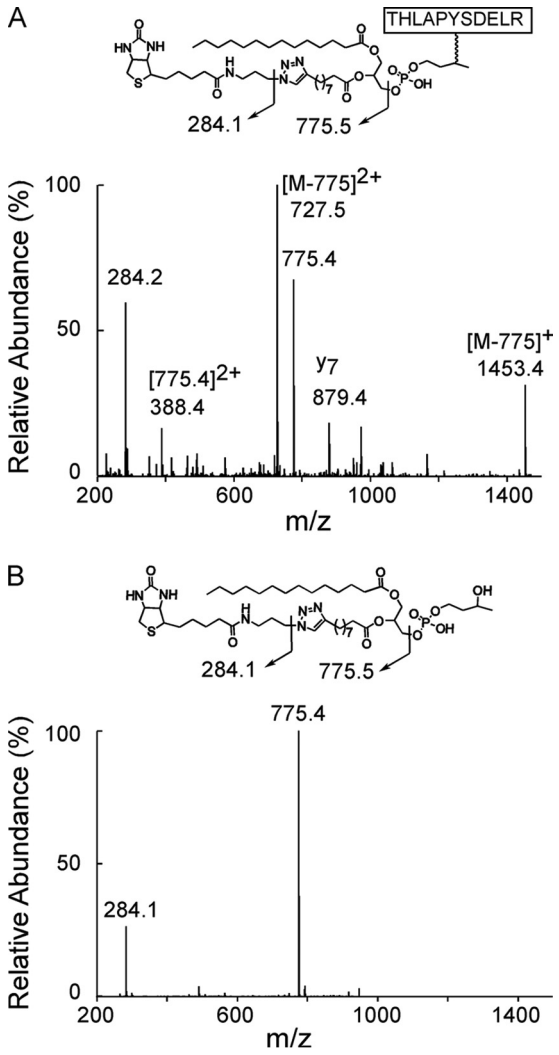

FIGURE 3. **pac-PC-labeled peptides have unique fragmentation patterns derived from pac-PC.** *A,* one representative tandem mass spectrum of pac-PC-modified apoA-I peptide (Thr_{161}-Arg_{171}) having the diagnostic fragments *m/z* 284 and *m/z* 775. *B,* tandem mass spectrum of pac-PC after photoactivation (in PBS buffer) and click chemistry reaction, which has dominant fragments *m/z* 284 and *m/z* 775.

tra identified abundant spectra with specific daughter fragmentations (ions produced during MS/MS ionization), such as *m/z* 284 and *m/z* 775 (one example is given in Fig. 3*A*) (note: our method involves two wash steps, which removed non-labeled apoA-I protein and non-labeled apoA-I peptides, and it made the manual inspection of the raw spectra possible). Identical daughter fragmentations (*m/z* 284 and *m/z* 775) from different peptide spectra suggested that the daughter ions at *m/z* 284 and *m/z* 775 were derived from the same source, the lipid modification. To test our hypothesis, we performed a control experiment as illustrated in Fig. 4. The synthetic lipid analogue, pac-PC, was either incorporated into HDL (*i.e.* in the presence of protein), as outlined above, or incubated alone in buffer (PBS) and then exposed to UV irradiation. Samples were then incubated with biotin azide to enable click chemistry-based biotinylation, followed by on-bead trypsin digestion and LC/MS/MS analysis (Fig. 4). The pac-PC sample exposed to UV irradiation alone in buffer (without the presence of apoA1/HDL), during MS ionization, gave rise to *m/z* 284 and *m/z* 775 as major fragments, confirming that these daughter ions arise from the pac-PC moiety itself. Thus, the reasons for difficulty using the automated peptide sequencing was because the lipid-modified peptides gave dominant fragments from cleavage of the lipid instead of from the peptide backbone, complicating spectra interpretation and resulting in failed software searches.

To circumvent this problem, we added a simple base hydrolysis step to the end of the overall scheme depicted in Fig. 4, the rationale for which is illustrated in the scheme shown in Fig. 5*A*. The ester bonds in lipids are more base-sensitive than amide bonds in peptides; thus, base-catalyzed hydrolysis effectively removed the bulk of the lipid fatty acid side chains leaving a characteristic small modification group (glycerol phosphate, +226.061 atomic mass units). For base-treated samples, we therefore applied a static modification of +226.061 atomic mass units to each amino acid for peptide analyses, corresponding to a glycerol phosphate group, as described under "Experimental Procedures." We found that applying this static +226.061 atomic mass unit modification gave structurally informative and recognizable peptide backbone fragmentations (Fig. 5). Thus, base-treated peptides were easily identified and recognized with exact modification sites by SEQUEST. As expected, examination of peptide spectra from pac-PC-containing rHDL showed that numerous residues throughout the length of apoA1 may be covalently tagged by pac-PC (one example is given in Fig. 5).

Use of rHDL Incorporating pac-PC to Identify PON1 Residues Involved in Binding to the HDL Lipid Surface—Having refined the above sample processing and mass spectrometry analyses using this new tool, we next applied it to the study of HDL-PON1 interaction, a test case to validate the utility of pac-PC in defining HDL-associated protein contact sites. A step by step scheme depicting the overall steps is shown in Fig. 6. Reconstituted nascent HDL incorporating low mol % (2%) pac-PC was prepared and then incubated with His-tagged rPON1 at 37 °C for 1 h. Cross-linking was performed as described under "Experimental Procedures" with brief (1 min) exposure to UV light (365 nm) at 0 °C. Proteins were precipitated, and then resolubilized rPON1 was enriched using Ni-NTA resin (to remove human apoA-I). Immobilized PON1-containing phospholipid adducts were biotinylated via click chemistry, and then lipid-tagged rPON1 was subjected to neutravidin enrichment and on-bead trypsin/chymotrypsin digestion (Fig. 6). Following a wash step to remove non-labeled peptides, the lipid-modified rPON1 peptides were eluted from the beads. After base treatment, facile identification of the modification sites on rPON1 was achieved by LC/MS/MS and searching for glycerol-phosphate modified peptides, which were detected by a static modification (+226.061) applied to each amino acid residue.

Three rPON1 peptides (Table 1) were reproducibly identified that carried the specific modification (+226.061) corresponding to the glycerol phosphate adduct (Ala_2-Lys_{21}, Ile_{291}-Lys_{297}, and Ala_{180}-Tyr-$_{190}$). The residue within each peptide (Leu-9, Tyr-185 and Tyr-293) carrying the glycerol-phosphate moiety derived from pac-PC is also shown, along with the excellent (within 10 ppm) agreement between the exact mass experimentally measured for each peptide and its theoretical mass based on elemental composition (Table 1). For illustrative pur-

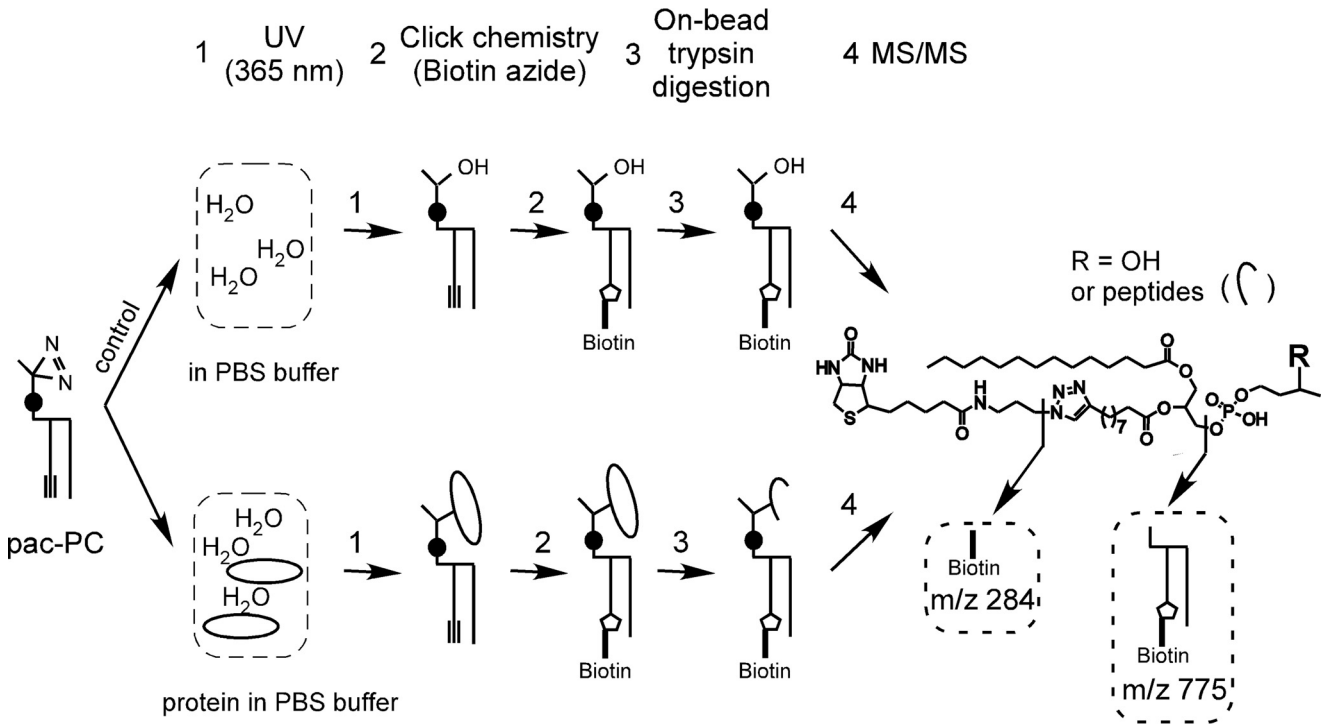

FIGURE 4. **Major MS/MS fragments of pac-PC-modified peptides come from lipid portion.** The control experiment was performed by using pac-PC vesicles in PBS buffer. For comparison, the steps for use and analysis of pac-PC-coupled peptides following interaction with protein (as in rHDL) are also shown. After UV irradiation, pac-PC is biotinylated through click chemistry and affinity-isolated, subjected to trypsinolysis, and analyzed by LC/MS/MS. In the example of only pac-PC exposed to UV irradiation in buffer alone, the final extracted lipid gave *m/z* 284 and *m/z* 775 as major MS/MS fragments, typical patterns from pac-PC-modified peptides. Thus, fragment ions *m/z* 284 and *m/z* 775 originate from the lipid portion of lipid-adducted peptides.

poses, the mass spectra of the native peptide Ile_{291}-Lys_{297} and the peptide Ile_{291}-Lys_{297} carrying the modification at residue Tyr-293 are presented in Fig. 7, *A* and *B*, respectively. Note that a static mass shift of +226 is observed on related b and y ions labeled with * in Fig. 7*B*. Also shown (Fig. 8) is the crystal structure for PON1 (73) with superimposed locations of Leu-9, Tyr-185, and Tyr-293, which collectively identify the interfacial surface that binds to the HDL particle. Of interest, PON1 Tyr-71, a residue we previously showed was in close spatial proximity to cholesterol within PON1 bound to an HDL particle using a photoaffinity-labeled cholesterol analogue (31), is similarly localized close to the identified HDL-binding interface (Fig. 8). Also of interest and discussed below, PON1 Tyr-294, despite being within ~5 Å with Tyr-293 (α-carbon to α-carbon; Fig. 8), failed to show pac-PC probe adduct formation in PON1-bound HDL, illustrating the remarkable specificity of residue interaction and covalent modification by the phospholipid photoactivatable group in the PON1-HDL complex.

As noted above, the rPON1 variant used in this study, G3C9, has two adjacent tyrosine residues (Tyr-293 and Tyr-294) in peptide Ile_{291}-Lys_{297}, but sequence analyses of affinity-isolated peptides recovered from PON1-HDL complexes following photoactivation of the pac-PC probe repeatedly showed only PON1 Tyr-293 was covalently adducted to the probe. To confirm that the lipid cross-link was at Tyr-293 instead of Tyr-294, we performed the more sensitive analysis of selected ion monitoring (*m/z* 586.3, corresponding to the lipid cross-linked peptide Ile_{291}-Lys_{297}) and collected its daughter fragments. We were able to successfully isolate a peptide that has the same *m/z* value but slightly different retention time, shown as the small shoulder peak (*peak 1*) on the chromatogram (Fig. 9*A*). This less abundant peptide, Ile_{291}-Lys_{297}, was observed to carry the lipid modification at Tyr-294 instead of Tyr-293, based on its MS/MS fragments (Fig. 9*B*; adduct at Tyr-294 is estimated to occur at a 10–20-fold reduced level compared with adduct at Tyr-293).

PON1 Residues Leu-9, Tyr-185, and Tyr-293 Are Functionally Important for HDL Binding and Preservation of PON1 Activity—To examine the functional significance of PON1 residues discovered as HDL lipid-binding sites (Leu-9, Tyr-185, and Tyr-293), we generated site-specific rPON1 mutants. All mutants were compared with the recombinant PON1 variant G3C9 (wild type-like activity, rPON1 WT). Residues (Leu-9, Tyr-185, and Tyr-293) were mutated to either glutamic acid (rPON1 pan-E) or lysine (rPON1 pan-K). The purified rPON1 mutants (pan-E or pan-K mutants) were observed to be homogeneous and have similar molecular weight, as shown by SDS-PAGE (Fig. 10*A*). Moreover, secondary structure analyses, as shown by circular dichroism (CD) spectra, revealed minimal differences when compared with WT rPON1 (Fig. 10*B*). We examined the catalytic activities of WT rPON1 and these rPON1 mutants by using paraoxon (paraoxonase activity) or phenyl acetate (arylesterase activity) as substrates. Purified rPON1 pan-K mutant demonstrated a specific activity of ~50% paraoxonase activity and ~80% arylesterase activity compared with rPON1 WT, whereas rPON1 pan-E mutant demonstrated almost complete loss of activity with either substrate (Fig. 11, *A* and *B*).

We interrogated the functional significance of PON1 residues Leu-9, Tyr-185 and Tyr-293 in HDL docking interactions

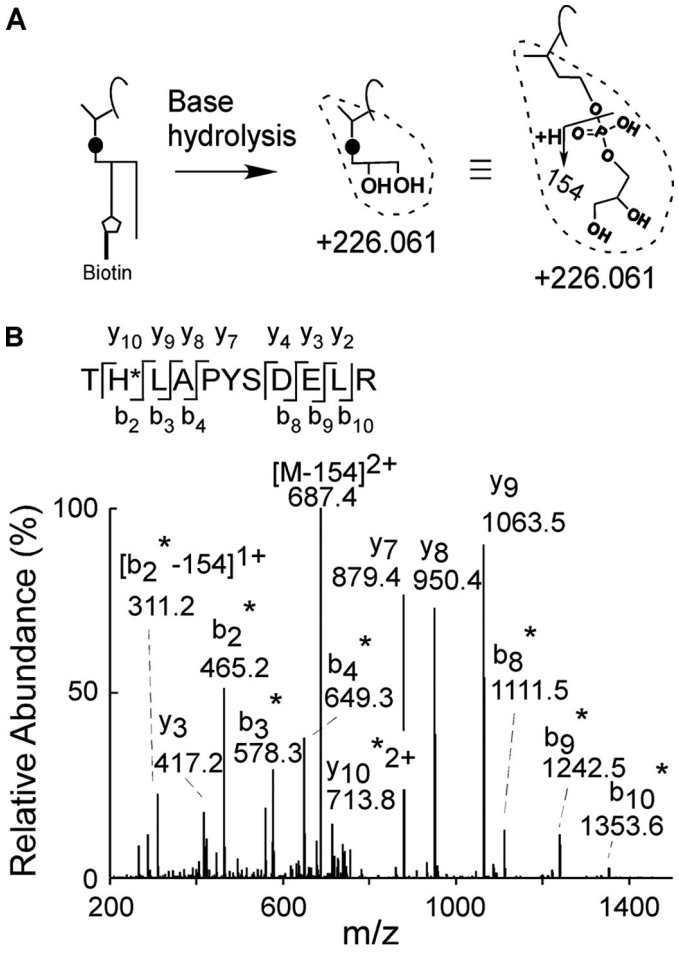

FIGURE 5. **Simple base hydrolysis step effectively removes the bulk of the lipid side delivering structurally informative and recognizable peptide backbone fragmentations.** Tandem mass spectrum of pac-PC modified apoA-I peptide (Thr-161–Arg-171) after base hydrolysis. Amino acid and b/y ions that carry hydrolyzed pac-PC modification group (+226.061) are labeled with *.

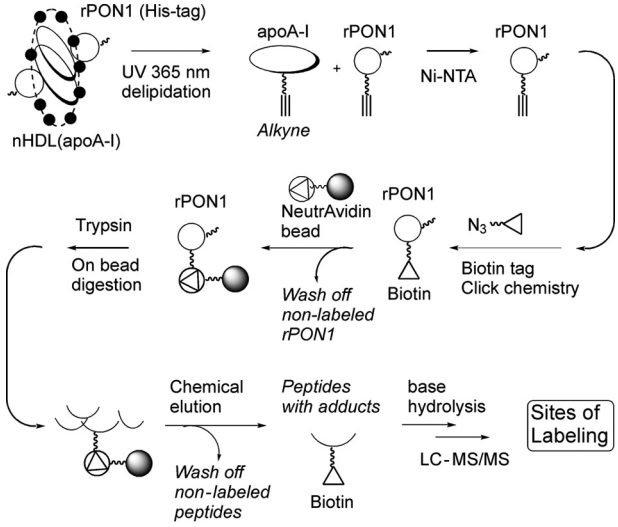

FIGURE 6. **Experimental scheme using pac-PC to investigate pac-PC-rPON1 interactions.** rHDL incorporating the 2 mol % pac-PC was incubated with His-tagged rPON1, and cross-linking was performed with brief exposure to UV light (365 nm) and enriched by using Ni-NTA resin as described under "Experimental Procedures." Immobilized PON1-containing phospholipid adducts were biotinylated via click chemistry and purified using neutravidin, digested with trypsin, and processed as described in Fig. 2. Lipid adducted-modified rPON1 peptides were eluted from the beads and base-treated to remove bulk lipid and allow facile identification of the modification sites on rPON1 by LC/MS/MS and searching for glycerol-phosphate-modified peptides, which were detected by a static modification (+226.061) applied to each amino acid residue. Details are described under "Experimental Procedures."

TABLE 1

Identified rPON1 residues that cross-linked with the photoactivatable lipid probe pac-PC

Three rPON1 peptides were reproducibly identified that carried the specific modification (+226.061) corresponding to the glycerol phosphate adduct. The residue within each peptide (Leu-9, Tyr-185, and Tyr-293) carrying the glycerol-phosphate moiety derived from pac-PC is also shown, along with the excellent (within 10 ppm) agreement between the exact mass experimentally measured for each peptide and its theoretical mass based on elemental composition. Mass spectra were originally filtered by XCorr (cross-correlation value) and were examined by manual inspection.

Labeled peptide	Labeled residue	$[M + H]^+$	ΔM	X-Corr
			ppm	
^{2}AKLTALTL*LGLGLALFDGQK^{21}	Leu-9	2269.2962	4.70	4.57
^{291}IFY*YDPK^{297}	Tyr-293	1171.5417	4.18	2.29
^{180}ATNDHY*FADPY^{190}	Tyr-185	1539.6117	5.07	2.51

by directly quantifying the collective role of the PON1 residues in binding to the HDL particle surface. For these studies, the binding of WT rPON1 (G3C9) and both mutant rPON1 forms (pan-E and pan-K) with rHDL were examined using surface plasmon resonance spectroscopy. Reconstituted HDL particles were directly coated on the sensor chips, and then diluted rPON1 solutions of different concentrations were individually flowed over the immobilized rHDL. Measured k_{on}, k_{off}, and K_d values for each PON1 form interaction with rHDL are shown in Table 2, and for illustrative purposes, typical binding sensorgrams for binding of rPON1 WT or rPON1 pan-K to rHDL are presented in Fig. 12, *A* and *B*, respectively. Of note, the rPON1 pan-K mutant showed 1000-fold less binding capacity to rHDL compared with rPON1 WT (K_d, 1.4×10^{-6} *versus* 7.1×10^{-10}, respectively, see Table 2). The rPON1 pan-E mutant showed even lower HDL binding capacity compared with the rPON1 pan-K mutant (K_d, 5.9×10^{-5} *versus* 1.4×10^{-6}, respectively, see Table 2). These results show that PON1 Leu-9, Tyr-185, and Tyr-293 participate in PON1-HDL interactions, and the nature of the site-specific mutations impact the affinity of the PON1 form to bind to HDL.

PON1 binding to HDL is known to stabilize PON1 catalytic activity at 37 °C, with both protein (apoA-I) and lipid phase of HDL contributing to the overall docking and stabilization of PON1 on the HDL particle (31, 74, 75). We therefore next analyzed the importance of PON1 Leu-9, Tyr-185, and Tyr-293 in PON1 stabilization with HDL particles. To speed inactivation, rPON1 (WT *versus* pan-K form) was incubated with a calcium chelator (EDTA) and a reducing agent, β-mercaptoethanol, in the presence or absence of rHDL or detergent (0.1% tergitol (Nonidet P-10)), and the rate of inactivation of PON1 was determined by monitoring arylesterase activity, as outlined under "Experimental Procedures" (Fig. 13, *A* and *B*). This approach has previously been used to examine and characterize human and rabbit PON activity stabilities (76, 77). A very slow inactivation of WT rPON1 was observed in the presence of rHDL (Fig. 13*A*), consistent with previous reports that HDL

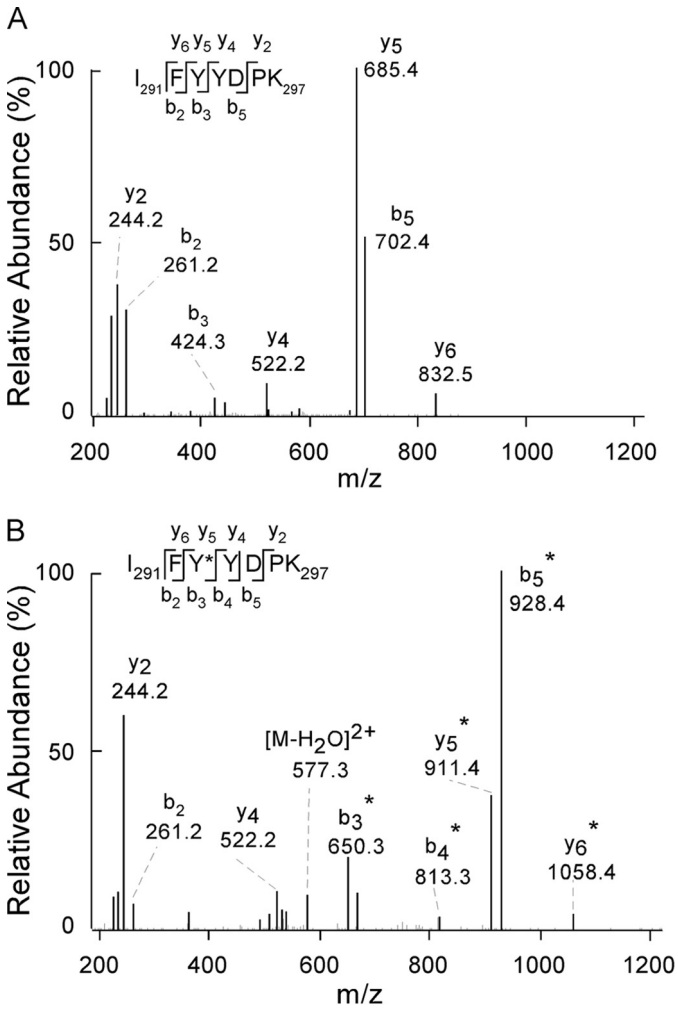

FIGURE 7. **Illustration of tandem mass spectra from rPON1 peptide Ile-291–Lys-297 and its cross-linking product with pac-PC.** The tandem mass spectra shown are rPON1 peptide Ile-291–Lys-297 (*A*) and rPON1 peptide Ile-291–Lys-297 (*B*), carrying a modification (+226.061) at Tyr-293. The pac-PC-modified amino acid and related b, y ions are labeled with *.

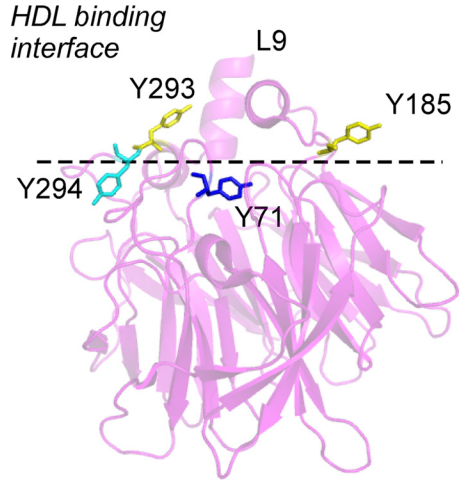

FIGURE 8. **Crystal structure of rPON1 with highlighted residues that cross-linked with photoactivatable lipid probes.** Shown is an image of human PON1 crystal structure (Protein Data Bank code 3SRE), with residues participating in the HDL-binding interface highlighted. Leu-9 (which is not shown on the structure), Tyr-185, and Tyr-293 (*yellow*) were identified that cross-linked with pac-PC. Tyr-294 (*cyan*) was later identified that also cross-linked with pac-PC but with much lower abundance (less than 5%) compared with Tyr-293, using the selective ion monitoring mode. Tyr-71 (*blue*) was previously identified in cross-linking experiments. All of these residues are located in the hypothetical HDL binding domain (above the *dashed line*, according to PON1 crystal structure and hydropathy analyses).

particles stabilize PON1 activity (77). Addition of detergent (0.1% tergitol, Nonidet P-10) to WT rPON1 showed an intermediate rate of inactivation, whereas rPON1 incubated with buffer alone showed a relatively rapid decay in activity (Fig. 13*A*). In contrast, no protective effects were observed when the pan-K rPON1 mutant was incubated with either rHDL or detergent (0.1% tergitol, Nonidet P-10), suggesting PON1 Leu-9, Tyr-185, and Tyr-293 additionally contribute to the HDL-dependent stabilization of PON1 activity to thermal denaturation and detergents.

Because PON1 Tyr-293 is photo-labeled by pac-PC to a greater extent (estimated 10–20-fold) compared with the adjacent Tyr-294 residue, we decided to assess the functional significance of each residue to HDL binding/stabilization of PON1 activity. PON1 Tyr-293 and Tyr-294 were individually mutated to Lys, and their PON1 activity (measured as arylesterase activity) was determined (Fig. 14*A*). PON1 Y293K and Y294K both possess catalytic activity. Interestingly, the specific activity of freshly isolated Y294K mutant appears modestly reduced compared with the WT and Y293K forms of the enzyme. To explore the strength and functional impact of the HDL-PON1 interaction with each PON1 residue, we further examined the stability of each mutant (Y293K *versus* Y294K) to inactivation in the presence or absence of rHDL, because both our studies (Fig. 13) and those of others (76, 77) show this is an excellent functional readout of the PON1-HDL interaction. Incubation of all PON1 forms (either WT or both mutants) in buffer containing EDTA and β-mercaptoethanol at 37 °C without HDL resulted in rapid loss of activity (data not shown). However, in the presence of HDL, the rate of PON1 inactivation in the WT *versus* mutant PON1 forms was markedly different and followed the order Y293K > Y294K ≫ WT (Fig. 14*B*). WT PON1 was completely stabilized to inactivation by binding to HDL over the time course examined. In contrast, Y293K was inactivated much faster and was less stabilized by HDL than the Y294K mutant, which showed intermediate deactivation rate (Fig. 14). These results are consistent with the pac-PC labeling studies, which suggest PON1 Tyr-293 plays a more significant role in PON1-HDL binding than PON1 Tyr-294 (because the extent of pac-PC labeling of Tyr-293 was 10–20-fold greater than Tyr-294).

Discussion

This study is significant for two distinct reasons. First, in general terms, it describes the development and characterization of a novel photoactivatable, affinity-taggable (via click chemistry), phospholipid probe (pac-PC) and the necessary sample processing and mass spectrometry-based analytical platform amenable for the facile discovery of specific residues on proteins involved in docking to phospholipid surfaces. Importantly, in addition to the inherent specificity and affinity enrichment steps enabled by the probe design, the sample processing and analyses methodology developed enables existing mass spectrometry software programs to be used for automated

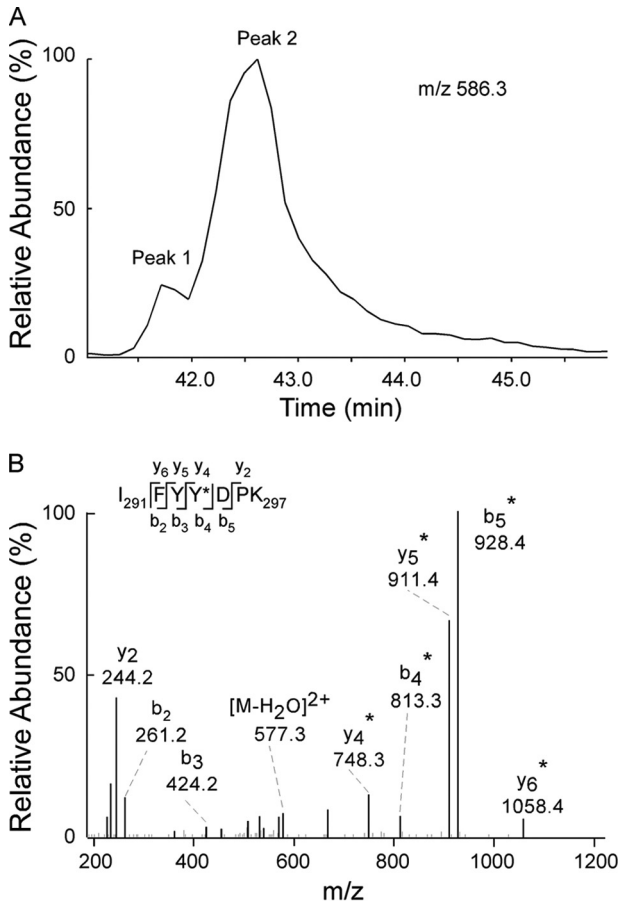

FIGURE 9. **Significant differences in cross-linking formation between pac-PC/Tyr-293 *versus* pac-PC/Tyr-294 demonstrate the spatial sensitivity and specificity of using pac-PC to interrogate lipid-protein interactions at the interface of PON1 and HDL.** *A,* chromatogram of the selective ion monitoring *m/z* 586.3 corresponding to rPON1 peptide Ile-291–Lys-297 carrying hydrolyzed pac-PC modification group (+226.061). A new peptide that has the same *m/z* value but slightly different retention time was isolated as the small shoulder peak (*peak 1*) on the chromatogram. *B,* new isolated tandem mass spectrum of rPON1 peptide Ile-291–Lys-297 carrying hydrolyzed pac-PC modification group (+226.061) at Tyr-294.

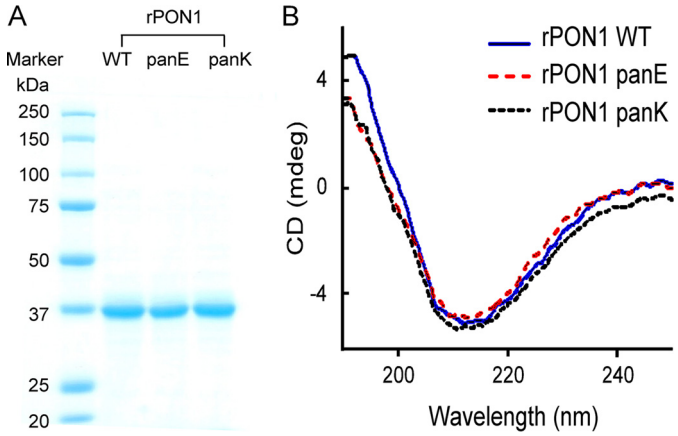

FIGURE 10. **Characterizations of site-specific rPON1 mutants.** All mutants were compared with the recombinant PON1 variant G3C9 (wild type like activity, rPON1 WT). Residues (Leu-9, Tyr-185 and Tyr-293) were mutated to either glutamic acid (rPON1 pan-E) or lysine (rPON1 pan-K). *A,* purified rPON1 WT, pan-E, and pan-K proteins were fractionated by 12% SDS-PAGE and stained with Coomassie Blue. *B,* circular dichroism spectra of purified rPON1 WT, pan-E, and pan-K proteins. rPON1 forms (WT, pan-E, and pan-K mutants) were analyzed at ambient temperature in continuous scan mode with a 1-nm bandwidth (100,000 counts/step). Details are described under "Experimental Procedures."

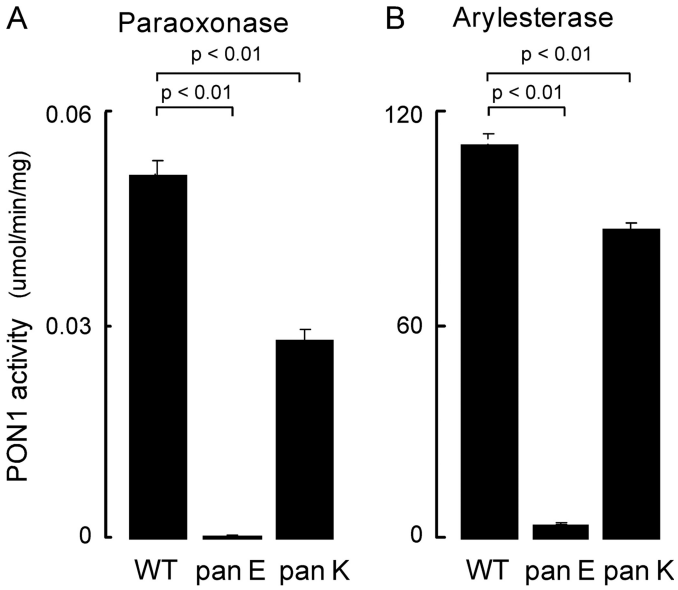

FIGURE 11. **PON1 residues Leu-9, Tyr-185, and Tyr-293 are functionally important for preservation of PON1 activity.** *A,* paraoxonase activity; *B,* arylesterase activity of purified rPON1 WT, pan-E, and pan-K mutants. Purified rPON1 pan-K mutant demonstrated a specific activity of ~50% paraoxonase activity and ~80% arylesterase activity compared with rPON1 WT, whereas rPON1 pan-E mutant demonstrated almost complete loss of activity with either substrate. Data shown represent the mean ± S.D. of triplicate determinations.

peptide identification, a significant advance over existing lipid photoactivatable probes. Second, on a more specific level, use of the novel probe, pac-PC, when incorporated into rHDL for proof of concept studies, helped to define three key residues on PON1 involved in HDL docking and stabilization of PON1 catalytic activity (Leu-9, Tyr-185, and Tyr-293).

In prior studies, we sought to define precise residues on PON1 that are involved in interaction with HDL cholesterol by incorporating a synthetic photoactivatable cholesterol analogue containing a diazirine moiety at C6 of the sterol into nascent HDL (31). The diazirine group, because of its position and hydrophilicity, is predicted to predominantly be exposed at the surface of the HDL particle. Although one residue of PON1, Tyr-71 (Fig. 8), was discovered in these early studies, the laborious mass spectrometry analyses required to detect a cholestanyl adduct within a sea of PON1 peptides was a major limitation of the approach. The absence of an affinity tag resulted in extremely low abundance of photolabeled peptides (one in ten thousand to million), making their identification tedious and extremely difficult. The new tool developed herein has numerous advantages. Importantly, it couples the specificity of a very short lived diradical intermediate upon photoactivation with a suitable affinity tag for enrichment (alkyne-azide-driven click chemistry to biotinylate). During the preparation of this study, a photoactivatable cholesterol probe with an affinity tag was reported and applied to globally map cholesterol-protein interactions in living cells (72). Instead, we designed a totally different photoactivatable probe (an analogue of phosphatidylcholine) to investigate protein-membrane or lipoprotein interactions. We originally chose to synthesize and characterize

TABLE 2

The binding affinities between rPON1 mutants (WT, pan-E, and pan-K) and recombinant nascent HDL particles through surface plasmon resonance

Recombinant nascent HDL was directly immobilized on a CM5 sensor chip. Samples of the indicated rPON1 ranging from 500 to 2000 nM were prepared in PON1 activity buffers (50 mM Tris, 50 mM NaCl, 1 mM $CaCl_2$, pH 8.0) and flowed over the surface of the sensor chip at a flow rate of 20 μl/min. The association constant rate (k_{on}), dissociation constant rate (k_{off}), and apparent dissociation constants (K_d) are listed in the table.

rPON1	Peptides with mutated amino acids	k_{on} (1/ms)	k_{off} (1/s)	K_d (1/M)
WT	^{2}AKLTALT**L**LGLGLALFDGQK^{21} ^{291}IF**Y**YDPK^{297} ^{180}ATNDH**Y**FADPY^{190}	1.2×10^{3}	8.5×10^{-7}	7.1×10^{-10}
pan-E	^{2}AKLTALT**E**LGLGLALFDGQK^{21} ^{291}IF**E**YDPK^{297} ^{180}ATNDH**E**FADPY^{190}	850	5.0×10^{-2}	5.9×10^{-5}
pan-K	^{2}AKLTALT**K**LGLGLALFDGQK^{21} ^{291}IF**K**YDPK^{297} ^{180}ATNDH**K**FADPY^{190}	42	6.0×10^{-5}	1.4×10^{-6}

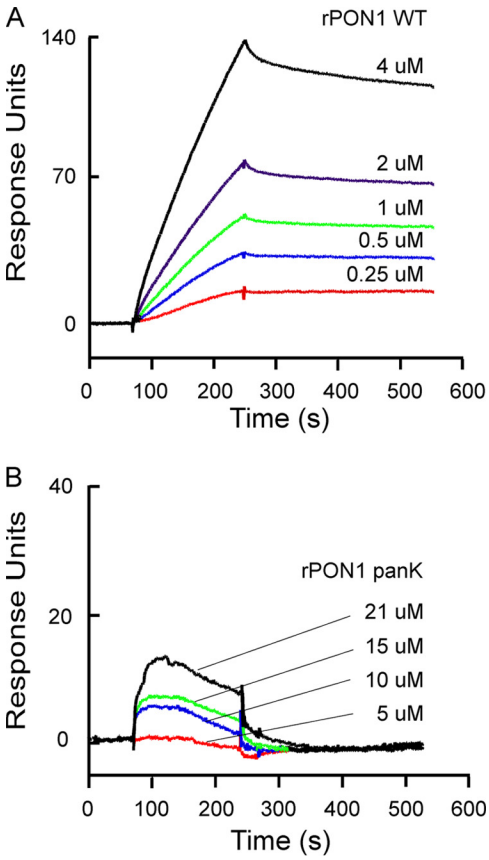

FIGURE 12. **PON1 residues Leu-9, Tyr-185, and Tyr-293 are functionally important for HDL binding.** Surface plasmon resonance sensorgrams of the binding of various concentrations of rPON1 are shown. *A*, WT; *B*, pan-K mutant to rHDL particles. rHDL was directly immobilized on a CM5 sensor chip. Samples of rPON1 ranging from 500 to 2000 nM were prepared in PON1 activity buffers and flowed over the surface of the sensor chip as described under "Experimental Procedures." The apparent dissociation constants (K_d) were obtained by fitting background-subtracted SPR binding data to the 1:1 binding with drifting baseline model within the BIAevaluation software version 4.0.

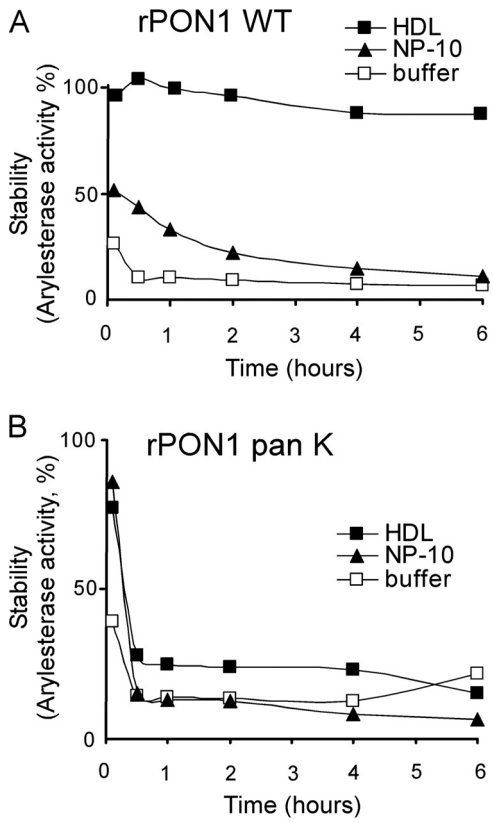

FIGURE 13. **PON1 residues Leu-9, Tyr-185, and Tyr-293 are functionally important to promote PON1 stabilization.** Kinetics of the inactivation of rPON1 WT (*A*) pan-K (*B*) in the solution of excess rHDL particles, 0.1% tergitol, or buffer only are shown. Recombinant PON1 WT and pan-K were preincubated with rHDLs (excess), 0.1% tergitol (*NP-10*), or PON1 activity buffer. Inactivation was initiated by adding an equal volume of denaturing buffer and incubating the samples as described under "Experimental Procedures." Aliquots were taken at the indicated time points, and arylesterase activities were examined. Data shown represent the mean ± S.D. of triplicate determinations.

this probe design due to the simplicity of its chemical structure and the relatively similar van der Waals size of the diazirine ring *versus* the trimethylamine of the choline headgroup moiety. We also recognized that pac-PC is convenient to chemically synthesize, and early control studies indicated it was stable enough under ambient light exposure to simplify its use. Later, during the mass spectrometry analysis of cross-linked peptide adducts, we found an unexpected advantage of this new probe that greatly enhances its potential utility, *i.e.* its ability to be used with commercial platform peptide sequencing software. Specifically, although the initial mass spectra obtained of lipid-adducted peptides were not easily recognized by current data analysis programs, addition of a base-hydrolysis step to remove the bulky lipid side chains was found to simplify automated data acquisition. Thus, using pac-PC under the methodology developed herein, mass spectra of glycerophosphate-tethered peptides are readily recognized by extant state of the art data anal-

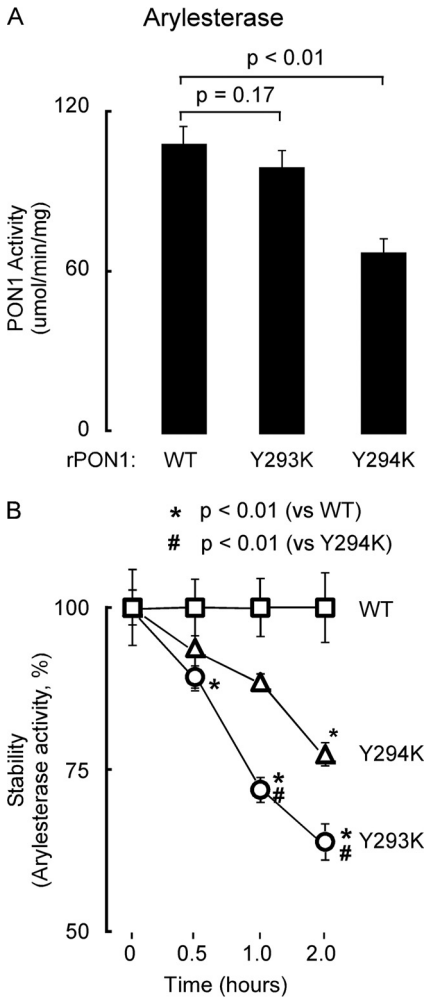

FIGURE 14. **PON1 adjacent residues Tyr-293 and Tyr-294 play different roles in PON1 activity and stabilization of PON1 through HDL interaction.** *A,* arylestrase activity of rPON1 WT, Y293K, and Y294K mutants in the presence of rHDL are shown. *B,* kinetics of the inactivation of rPON1 WT, Y293K, and Y294K mutants in the presence of excess HDL particles is shown. rPON1WT, Y293K, and Y294K were preincubated with rHDLs as described under "Experimental Procedures," and inactivation was initiated by adding an equal volume of denaturing buffer (containing metal chelator and reducing agent) and incubating the samples at 37 °C as described under "Experimental Procedures." Aliquots were taken at the indicated time points, and arylesterase activity in reactions was determined. Data shown represent the mean ± S.D. of triplicate determinations.

ysis programs (*e.g.* SEQUEST) by applying a static modification of +226.061 atomic mass units to each amino acid for peptide analyses. This feature of the present methodology is unique, and it markedly simplifies the identification process of affinity-tagged peptides and the critical residue(s) involved in lipid adduct formation.

Some potential limitations about pac-PC are worth noting. The current probe design for pac-PC will likely preferentially recognize a subset of residues on a docking protein, such as those that are involved with the initial interaction at or near a membrane surface or lipoprotein interface. Indeed, it is possible that the pac-PC design developed may not optimally interrogate regions of lipid-binding proteins that penetrate far into the acyl chain region of membrane bilayers or lipoproteins. Based upon the methodology developed herein, however, one can reasonably envision future development of alternative pac-PC analogues where the diazirine group (or alternative photoactivatable moiety) is placed at different positions along one of the fatty acyl side chains to probe residues on docking proteins that penetrate to greater depths of a hydrophobic surface. Base hydrolysis of these would generate peptides adducted to the fatty acyl moiety harboring the diazirine group. Similarly, incorporation of the photo-affinity group into phospholipids of alternative classes (headgroups), and thus potential biological functionality, might further expand the utility of these tools.

In our current application of probing the PON1-HDL interface, visual inspection of the location of the PON1 residues identified (Leu-9, Tyr-185 and Tyr-293) shows they are all localized in close vicinity to a hypothetical PON1 hydrophobic binding surface based upon a recently reported PON1 crystal structure and hydropathy analyses (Fig. 8) (73). Of note, residue Leu-9 is close to the N terminus of rPON1, which was not visualized in the crystal structure. However, the N-terminal helix (helix 1) of PON1 has previously been suggested to play an important role in PON1-HDL interaction based upon deletion mutant studies. Specifically, the recombinant PON1 truncated variant (Δ20, lacking the first 20 amino acids) was reported to have much lower binding affinity for HDL particles compared with the full-length version (77). PON1 Tyr-185 is located on the loop adjacent to helix 2, whereas Tyr-293 is at the end of helix 3. However, they are all in relatively close spatial proximity and together define an interfacial docking surface for PON1 on HDL (Fig. 8). Prior studies have suggested helices 2 (Asp_{188}-Leu_{198}) and 3 (Asn_{287}-Tyr_{293}) may potentially participate in PON1-HDL interactions based on the analyses of the exposed hydrophobic surfaces on the PON1 crystal structure (73), yet no experimental validation nor specific residues in these regions have been examined for their functional significance in lipid binding. Interestingly, two hydrophobic residues (Tyr-190 and Trp-194) on helix 2, previously hypothesized to potentially be involved in HDL anchoring based on their hydrophobicity (73), were not identified to cross-link with the photo-lipid probe in this study despite extensive searches for these adducts. One possible explanation is that apoA-I of HDL may prevent contact between these PON1 residues and the photoactivatable lipid probe within the surface of the HDL particle. By using hydrogen-deuterium exchange mass spectrometry analysis, we previously identified two regions on apoA-I of nascent HDL that interact with PON1 (31), and these peptides are predicted to be in close spatial proximity (exactly opposite to each other on the anti-parallel apoA-I chains of nascent HDL) (78). Although speculative at present, it is conceivable that these residues on PON1 helix 2 may directly interact with the hydrophobic surface of one or both of these two anti-parallel regions of apoA-I, thus reducing their access to the phospholipid surface on HDL particles. Another possibility is simply that neither of the two PON1 hydrophobic residues (Tyr-190 and Trp-194) on helix 2 play a role in PON1-HDL interaction.

Our mutagenesis studies of PON1 Leu-9, Tyr-185, and Tyr-293 confirm their functional significance for PON1-HDL interaction. The identified phospholipid adducts with residues Tyr-185 and Tyr-293 are consistent with a role of at least portions of

helix 2 and 3 of PON1 functioning in the HDL interaction. These studies thus provide structural information for how these helix domains of PON1 are anchored to the HDL phospholipid surface (via PON1 Tyr-185 and Tyr-293). Interestingly, as shown in Fig. 8, the crystal structure of rPON1 (73) reveals that the two adjacent tyrosine residues we examined in detail (Tyr-293 and Tyr-294), although close, are positioned in opposite orientations. Tyr-293, which was more readily identified as a covalent adduct to the photo-affinity phospholipid probe (~20-fold greater), faces toward the hypothetical HDL lipid surface where it can support PON1 binding to the lipid HDL phase. In contrast, the crystal structure predicts Tyr-294 is oriented virtually 180° in the opposite direction away from the potential HDL-binding interface. Thus, despite the theoretically equivalent reactivity of the phenol moiety of each residue with a carbene diradical, and their close spatial proximity (the α-carbons of each Tyr are within 4.8 Å in the crystal structure (73)), significant differences in the ease of covalent adduct formation was noted between these residues. The markedly different orientation of the tyrosine residues likely explains this difference. This interesting finding also demonstrates the spatial sensitivity and specificity of our approach to interrogate lipid-protein interactions. It is also notable that our mutagenesis studies verified that the Y293K mutant was less stable to denaturation in the presence of HDL compared with either Y294K or WT PON1.

PON1 is an HDL-associated protein with cardioprotective functions (36, 37). Its antioxidant and anti-inflammatory effects have been extensively observed *in vitro* and *in vivo* (12, 31, 32, 36, 37, 79). Some pharmaceutical effort has even been aimed at developing PON1, or PON1-HDL complexes, as an injectable biological agent for various indications ranging from the treatment of exposure to organophosphate nerve agents to the prevention or treatment of cardiovascular diseases (80, 81). Progress in this arena has been hampered by poor stability of the injected PON1 into the systemic circulation, and it has been suggested that an improved understanding of specific structural features critical to PON1 docking to the HDL particle and that are functionally important for maintenance of PON1 stability and catalytic activity may assist in these endeavors (82, 83). This study may thus help with future therapeutic agent efforts using PON1.

Finally, our recent finding that PON1, myeloperoxidase, and HDL form a functional ternary complex *in vivo* (31) provides a unique perspective for the understanding of the cardioprotective functions of PON1. Myeloperoxidase is a leukocyte-derived heme protein that often initiates lipid peroxidation and protein oxidative damage during inflammation (43, 48, 84–87). The fact that PON1 binds to both myeloperoxidase and HDL on the HDL surface, partially inhibiting myeloperoxidase activity, was shown to also help PON1 inhibit initiation of lipid peroxidation by myeloperoxidase. Alternative studies have suggested the lactonase activity of PON1 contributes to its anti-oxidant activity through hydrolysis of specific lipid peroxidation products (88, 89). A better understanding of the critical residues supporting PON1 interactions with HDL may thus help better understand the mechanisms through which the protein exerts its anti-oxidant and cardioprotective effects. Further studies in this area seem warranted.

Author Contributions—X. G. performed the majority of the experiments and along with A. J. D. constructed the various mutant PON1s. X. G. and S. L. H. wrote the manuscript. S. L. H. conceived the project and X. G. and S. L. H. designed and supervised the studies. X. G., J. A. D., and S. L. H. analyzed the data. Y. H. assisted X. G. in performing the SPR experiments and in data analysis. A. J. D., L. B. H., and J. L. produced and helped purify recombinant proteins. B. S. L. made photoaffinity cross-linking probes along with X. G. G. G., V. G., and B. S. L performed LC/MS/MS experiments and data analysis. All authors reviewed the manuscript.

References

1. Gordon, T., Castelli, W. P., Hjortland, M. C., Kannel, W. B., and Dawber, T. R. (1977) High density lipoprotein as a protective factor against coronary heart disease. The Framingham Study. *Am. J. Med.* **62,** 707–714
2. Fisher, E. A., Feig, J. E., Hewing, B., Hazen, S. L., and Smith, J. D. (2012) High density lipoprotein function, dysfunction, and reverse cholesterol transport. *Arterioscler. Thromb. Vasc. Biol.* **32,** 2813–2820
3. Rosenson, R. S., Brewer, H. B., Jr., Ansell, B., Barter, P., Chapman, M. J., Heinecke, J. W., Kontush, A., Tall, A. R., and Webb, N. R. (2013) Translation of high density lipoprotein function into clinical practice: current prospects and future challenges. *Circulation* **128,** 1256–1267
4. Toth, P. P., Barter, P. J., Rosenson, R. S., Boden, W. E., Chapman, M. J., Cuchel, M., D'Agostino, R. B., Sr., Davidson, M. H., Davidson, W. S., Heinecke, J. W., Karas, R. H., Kontush, A., Krauss, R. M., Miller, M., and Rader, D. J. (2013) High density lipoproteins: a consensus statement from the National Lipid Association. *J. Clin. Lipidol.* **7,** 484–525
5. Rye, K. A., and Barter, P. J. (2014) Regulation of high density lipoprotein metabolism. *Circ. Res.* **114,** 143–156
6. Kontush, A., Lindahl, M., Lhomme, M., Calabresi, L., Chapman, M. J., and Davidson, W. S. (2015) Structure of HDL: particle subclasses and molecular components. *Handb. Exp. Pharmacol.* **224,** 3–51
7. Rosenson, R. S., Brewer, H. B., Jr., Davidson, W. S., Fayad, Z. A., Fuster, V., Goldstein, J., Hellerstein, M., Jiang, X. C., Phillips, M. C., Rader, D. J., Remaley, A. T., Rothblat, G. H., Tall, A. R., and Yvan-Charvet, L. (2012) Cholesterol efflux and atheroprotection: advancing the concept of reverse cholesterol transport. *Circulation* **125,** 1905–1919
8. Rader, D. J., and Hovingh, G. K. (2014) HDL and cardiovascular disease. *Lancet* **384,** 618–625
9. Vickers, K. C., and Remaley, A. T. (2014) HDL and cholesterol: life after the divorce? *J. Lipid Res.* **55,** 4–12
10. Besler, C., Heinrich, K., Rohrer, L., Doerries, C., Riwanto, M., Shih, D. M., Chroni, A., Yonekawa, K., Stein, S., Schaefer, N., Mueller, M., Akhmedov, A., Daniil, G., Manes, C., Templin, C., *et al.* (2011) Mechanisms underlying adverse effects of HDL on eNOS-activating pathways in patients with coronary artery disease. *J. Clin. Invest.* **121,** 2693–2708
11. Sorci-Thomas, M. G., and Thomas, M. J. (2012) High density lipoprotein biogenesis, cholesterol efflux, and immune cell function. *Arterioscler. Thromb. Vasc. Biol.* **32,** 2561–2565
12. Bhattacharyya, T., Nicholls, S. J., Topol, E. J., Zhang, R., Yang, X., Schmitt, D., Fu, X., Shao, M., Brennan, D. M., Ellis, S. G., Brennan, M. L., Allayee, H., Lusis, A. J., and Hazen, S. L. (2008) Relationship of paraoxonase 1 (PON1) gene polymorphisms and functional activity with systemic oxidative stress and cardiovascular risk. *JAMA* **299,** 1265–1276
13. Vickers, K. C., Palmisano, B. T., Shoucri, B. M., Shamburek, R. D., and Remaley, A. T. (2011) MicroRNAs are transported in plasma and delivered to recipient cells by high density lipoproteins. *Nat. Cell Biol.* **13,** 423–433
14. Zamanian-Daryoush, M., Lindner, D., Tallant, T. C., Wang, Z., Buffa, J., Klipfell, E., Parker, Y., Hatala, D., Parsons-Wingerter, P., Rayman, P., Yusufishaq, M. S., Fisher, E. A., Smith, J. D., Finke, J., DiDonato, J. A., and Hazen, S. L. (2013) The cardioprotective protein apolipoprotein A1 promotes potent anti-tumorigenic effects. *J. Biol. Chem.* **288,** 21237–21252

15. Tabet, F., Vickers, K. C., Cuesta Torres, L. F., Wiese, C. B., Shoucri, B. M., Lambert, G., Catherinet, C., Prado-Lourenco, L., Levin, M. G., Thacker, S., Sethupathy, P., Barter, P. J., Remaley, A. T., and Rye, K. A. (2014) HDL-transferred microRNA-223 regulates ICAM-1 expression in endothelial cells. *Nat. Commun.* **5,** 3292
16. Sag, D., Cekic, C., Wu, R., Linden, J., and Hedrick, C. C. (2015) The cholesterol transporter ABCG1 links cholesterol homeostasis and tumour immunity. *Nat. Commun.* **6,** 6354
17. Karlsson, H., Leanderson, P., Tagesson, C., and Lindahl, M. (2005) Lipoproteomics II: mapping of proteins in high density lipoprotein using two-dimensional gel electrophoresis and mass spectrometry. *Proteomics* **5,** 1431–1445
18. Heller, M., Stalder, D., Schlappritzi, E., Hayn, G., Matter, U., and Haeberli, A. (2005) Mass spectrometry-based analytical tools for the molecular protein characterization of human plasma lipoproteins. *Proteomics* **5,** 2619–2630
19. Hortin, G. L., Shen, R. F., Martin, B. M., and Remaley, A. T. (2006) Diverse range of small peptides associated with high density lipoprotein. *Biochem. Biophys. Res. Commun.* **340,** 909–915
20. Rezaee, F., Casetta, B., Levels, J. H., Speijer, D., and Meijers, J. C. (2006) Proteomic analysis of high density lipoprotein. *Proteomics* **6,** 721–730
21. Ståhlman, M., Davidsson, P., Kanmert, I., Rosengren, B., Borén, J., Fagerberg, B., and Camejo, G. (2008) Proteomics and lipids of lipoproteins isolated at low salt concentrations in D2O/sucrose or in KBr. *J. Lipid Res.* **49,** 481–490
22. Li, H., Gordon, S. M., Zhu, X., Deng, J., Swertfeger, D. K., Davidson, W. S., and Lu, L. J. (2015) Network-based analysis on orthogonal separation of human plasma uncovers distinct high density lipoprotein complexes. *J. Proteome Res.* **14,** 3082–3094
23. Vaisar, T., Pennathur, S., Green, P. S., Gharib, S. A., Hoofnagle, A. N., Cheung, M. C., Byun, J., Vuletic, S., Kassim, S., Singh, P., Chea, H., Knopp, R. H., Brunzell, J., Geary, R., Chait, A., *et al.* (2007) Shotgun proteomics implicates protease inhibition and complement activation in the antiinflammatory properties of HDL. *J. Clin. Invest.* **117,** 746–756
24. Davidson, W. S., Silva, R. A., Chantepie, S., Lagor, W. R., Chapman, M. J., and Kontush, A. (2009) Proteomic analysis of defined HDL subpopulations reveals particle-specific protein clusters: relevance to antioxidative function. *Arterioscler. Thromb. Vasc. Biol.* **29,** 870–876
25. Alwaili, K., Bailey, D., Awan, Z., Bailey, S. D., Ruel, I., Hafiane, A., Krimbou, L., Laboissiere, S., and Genest, J. (2012) The HDL proteome in acute coronary syndromes shifts to an inflammatory profile. *Biochim. Biophys. Acta* **1821,** 405–415
26. Gordon, S. M., Deng, J., Lu, L. J., and Davidson, W. S. (2010) Proteomic characterization of human plasma high density lipoprotein fractionated by gel filtration chromatography. *J. Proteome Res.* **9,** 5239–5249
27. Shah, A. S., Tan, L., Long, J. L., and Davidson, W. S. (2013) Proteomic diversity of high density lipoproteins: our emerging understanding of its importance in lipid transport and beyond. *J. Lipid Res.* **54,** 2575–2585
28. Birner-Gruenberger, R., Schittmayer, M., Holzer, M., and Marsche, G. (2014) Understanding high density lipoprotein function in disease: recent advances in proteomics unravel the complexity of its composition and biology. *Prog. Lipid Res.* **56,** 36–46
29. Chang, C. T., Yang, C. Y., Tsai, F. J., Lin, S. Y., and Chen, C. J. (2015) Mass spectrometry-based proteomic study makes high density lipoprotein a biomarker for atherosclerotic vascular disease. *Biomed. Res. Int.* **2015,** 164846
30. Shih, D. M., Gu, L., Hama, S., Xia, Y. R., Navab, M., Fogelman, A. M., and Lusis, A. J. (1996) Genetic-dietary regulation of serum paraoxonase expression and its role in atherogenesis in a mouse model. *J. Clin. Invest.* **97,** 1630–1639
31. Huang, Y., Wu, Z., Riwanto, M., Gao, S., Levison, B. S., Gu, X., Fu, X., Wagner, M. A., Besler, C., Gerstenecker, G., Zhang, R., Li, X. M., Didonato, A. J., Gogonea, V., Tang, W. H., *et al.* (2013) Myeloperoxidase, paraoxonase-1, and HDL form a functional ternary complex. *J. Clin. Invest.* **123,** 3815–3828
32. Mackness, M. I., Arrol, S., and Durrington, P. N. (1991) Paraoxonase prevents accumulation of lipoperoxides in low density lipoprotein. *FEBS Lett.* **286,** 152–154
33. Watson, A. D., Berliner, J. A., Hama, S. Y., La Du, B. N., Faull, K. F., Fogelman, A. M., and Navab, M. (1995) Protective effect of high density lipoprotein associated paraoxonase. Inhibition of the biological activity of minimally oxidized low density lipoprotein. *J. Clin. Invest.* **96,** 2882–2891
34. Aviram, M., Rosenblat, M., Bisgaier, C. L., Newton, R. S., Primo-Parmo, S. L., and La Du, B. N. (1998) Paraoxonase inhibits high density lipoprotein oxidation and preserves its functions. A possible peroxidative role for paraoxonase. *J. Clin. Invest.* **101,** 1581–1590
35. Mackness, M., and Mackness, B. (2015) Human paraoxonase-1 (PON1): Gene structure and expression, promiscuous activities and multiple physiological roles. *Gene* **567,** 12–21
36. Shih, D. M., Gu, L., Xia, Y. R., Navab, M., Li, W. F., Hama, S., Castellani, L. W., Furlong, C. E., Costa, L. G., Fogelman, A. M., and Lusis, A. J. (1998) Mice lacking serum paraoxonase are susceptible to organophosphate toxicity and atherosclerosis. *Nature* **394,** 284–287
37. Tward, A., Xia, Y. R., Wang, X. P., Shi, Y. S., Park, C., Castellani, L. W., Lusis, A. J., and Shih, D. M. (2002) Decreased atherosclerotic lesion formation in human serum paraoxonase transgenic mice. *Circulation* **106,** 484–490
38. Tang, W. H., Wu, Y., Mann, S., Pepoy, M., Shrestha, K., Borowski, A. G., and Hazen, S. L. (2011) Diminished antioxidant activity of high density lipoprotein-associated proteins in systolic heart failure. *Circ. Heart Fail.* **4,** 59–64
39. Tang, W. H., Hartiala, J., Fan, Y., Wu, Y., Stewart, A. F., Erdmann, J., Kathiresan, S., CARDIoGRAM Consortium, Roberts, R., McPherson, R., Allayee, H., and Hazen, S. L. (2012) Clinical and genetic association of serum paraoxonase and arylesterase activities with cardiovascular risk. *Arterioscler. Thromb. Vasc. Biol.* **32,** 2803–2812
40. Zhao, Y., Ma, Y., Fang, Y., Liu, L., Wu, S., Fu, D., and Wang, X. (2012) Association between PON1 activity and coronary heart disease risk: a meta-analysis based on 43 studies. *Mol. Genet. Metab.* **105,** 141–148
41. Kennedy, D. J., Tang, W. H., Fan, Y., Wu, Y., Mann, S., Pepoy, M., and Hazen, S. L. (2013) Diminished antioxidant activity of high density lipoprotein-associated proteins in chronic kidney disease. *J. Am. Heart Assoc.* **2,** e000104
42. Schmitt, D., Shen, Z., Zhang, R., Colles, S. M., Wu, W., Salomon, R. G., Chen, Y., Chisolm, G. M., and Hazen, S. L. (1999) Leukocytes utilize myeloperoxidase-generated nitrating intermediates as physiological catalysts for the generation of biologically active oxidized lipids and sterols in serum. *Biochemistry* **38,** 16904–16915
43. Zhang, R., Shen, Z., Nauseef, W. M., and Hazen, S. L. (2002) Defects in leukocyte-mediated initiation of lipid peroxidation in plasma as studied in myeloperoxidase-deficient subjects: systematic identification of multiple endogenous diffusible substrates for myeloperoxidase in plasma. *Blood* **99,** 1802–1810
44. Brennan, M. L., Penn, M. S., Van Lente, F., Nambi, V., Shishehbor, M. H., Aviles, R. J., Goormastic, M., Pepoy, M. L., McErlean, E. S., Topol, E. J., Nissen, S. E., and Hazen, S. L. (2003) Prognostic value of myeloperoxidase in patients with chest pain. *N. Engl. J. Med.* **349,** 1595–1604
45. Hazen, S. L. (2004) Myeloperoxidase and plaque vulnerability. *Arterioscler. Thromb. Vasc. Biol.* **24,** 1143–1146
46. Kalantar-Zadeh, K., Brennan, M. L., and Hazen, S. L. (2006) Serum myeloperoxidase and mortality in maintenance hemodialysis patients. *Am. J. Kidney Dis.* **48,** 59–68
47. Nicholls, S. J., and Hazen, S. L. (2009) Myeloperoxidase, modified lipoproteins, and atherogenesis. *J. Lipid Res.* **50,** S346–S351
48. Huang, Y., DiDonato, J. A., Levison, B. S., Schmitt, D., Li, L., Wu, Y., Buffa, J., Kim, T., Gerstenecker, G. S., Gu, X., Kadiyala, C. S., Wang, Z., Culley, M. K., Hazen, J. E., Didonato, A. J., *et al.* (2014) An abundant dysfunctional apolipoprotein A1 in human atheroma. *Nat. Med.* **20,** 193–203
49. Zheng, L., Nukuna, B., Brennan, M. L., Sun, M., Goormastic, M., Settle, M., Schmitt, D., Fu, X., Thomson, L., Fox, P. L., Ischiropoulos, H., Smith, J. D., Kinter, M., and Hazen, S. L. (2004) Apolipoprotein A-I is a selective target for myeloperoxidase-catalyzed oxidation and functional impairment in subjects with cardiovascular disease. *J. Clin. Invest.* **114,** 529–541
50. Still, W. C., Kahn, M., and Mitra, A. (1978) Rapid chromatographic technique for preparative separations with moderate resolution. *J. Org. Chem.* **43,** 2923–2925
51. Markwell, M. A., Haas, S. M., Bieber, L. L., and Tolbert, N. E. (1978) A

modification of the Lowry procedure to simplify protein determination in membrane and lipoprotein samples. *Anal. Biochem.* **87,** 206–210
52. Church, R. F., and Weiss, M. J. (1970) Diazirines. 11. synthesis and properties of small functionalized Diazirine molecules. Some observations on the reaction of a Diaziridine with the iodine-iodide ion system. *J. Org. Chem.* **35,** 2465–2471
53. Schmitz, E., and Ohme, R. (1965) 3,3-Pentamethylenediazirine. *Organic Syntheses Collective Volume* **5,** 83
54. Bligh, E. G., and Dyer, W. J. (1959) A rapid method of total lipid extraction and purification. *Can. J. Biochem. Physiol.* **37,** 911–917
55. Havel, R. J., Eder, H. A., and Bragdon, J. H. (1955) The distribution and chemical composition of ultracentrifugally separated lipoproteins in human serum. *J. Clin. Invest.* **34,** 1345–1353
56. Osborne, J. C., Jr. (1986) Delipidation of plasma lipoproteins. *Methods Enzymol.* **128,** 213–222
57. Rye, K. A., Garrety, K. H., and Barter, P. J. (1992) Changes in the size of reconstituted high density lipoproteins during incubation with cholesteryl ester transfer protein: the role of apolipoproteins. *J. Lipid Res.* **33,** 215–224
58. Matz, C. E., and Jonas, A. (1982) Micellar complexes of human apolipoprotein A-I with phosphatidylcholines and cholesterol prepared from cholate-lipid dispersions. *J. Biol. Chem.* **257,** 4535–4540
59. Baker, P. W., Rye, K. A., Gamble, J. R., Vadas, M. A., and Barter, P. J. (2000) Phospholipid composition of reconstituted high density lipoproteins influences their ability to inhibit endothelial cell adhesion molecule expression. *J. Lipid Res.* **41,** 1261–1267
60. Aharoni, A., Gaidukov, L., Yagur, S., Toker, L., Silman, I., and Tawfik, D. S. (2004) Directed evolution of mammalian paraoxonases PON1 and PON3 for bacterial expression and catalytic specialization. *Proc. Natl. Acad. Sci. U.S.A.* **101,** 482–487
61. Hannoush, R. N., and Arenas-Ramirez, N. (2009) Imaging the lipidome: omega-alkynyl fatty acids for detection and cellular visualization of lipid-modified proteins. *ACS Chem. Biol.* **4,** 581–587
62. Weerapana, E., Speers, A. E., and Cravatt, B. F. (2007) Tandem orthogonal proteolysis-activity-based protein profiling (TOP-ABPP)–a general method for mapping sites of probe modification in proteomes. *Nat. Protoc.* **2,** 1414–1425
63. Speers, A. E., and Cravatt, B. F. (2005) A tandem orthogonal proteolysis strategy for high content chemical proteomics. *J. Am. Chem. Soc.* **127,** 10018–10019
64. Eng, J. K., McCormack, A. L., and Yates, J. R. (1994) An approach to correlate tandem mass spectral data of peptides with amino acid sequences in a protein database. *J. Am. Soc. Mass Spectrom.* **5,** 976–989
65. Tabb, D. L., McDonald, W. H., and Yates, J. R., 3rd. (2002) DTASelect and Contrast: tools for assembling and comparing protein identifications from shotgun proteomics. *J. Proteome Res.* **1,** 21–26
66. Das, J. (2011) Aliphatic diazirines as photoaffinity probes for proteins: recent developments. *Chem. Rev.* **111,** 4405–4417
67. Rostovtsev, V. V., Green, L. G., Fokin, V. V., and Sharpless, K. B. (2002) A stepwise huisgen cycloaddition process: copper(I)-catalyzed regioselective "ligation" of azides and terminal alkynes. *Angew. Chem. Int. Ed. Engl.* **41,** 2596–2599
68. Best, M. D., Rowland, M. M., and Bostic, H. E. (2011) Exploiting bioorthogonal chemistry to elucidate protein-lipid binding interactions and other biological roles of phospholipids. *Acc. Chem. Res.* **44,** 686–698
69. Pajouhesh, H., and Hancock, A. J. (1983) Synthesis of conformationally restricted acidic lipids. I. Cyclopentanoid analogs of phosphatidylserine. *J. Lipid Res.* **24,** 645–651
70. Menashe, M., Romero, G., Biltonen, R. L., and Lichtenberg, D. (1986) Hydrolysis of dipalmitoylphosphatidylcholine small unilamellar vesicles by porcine pancreatic phospholipase A2. *J. Biol. Chem.* **261,** 5328–5333
71. Gu, X., Zhang, W., Choi, J., Li, W., Chen, X., Laird, J. M., and Salomon, R. G. (2011) An (1)O2 route to gamma-hydroxyalkenal phospholipids by vitamin E-induced fragmentation of hydroperoxydiene-derived endoperoxides. *Chem. Res. Toxicol.* **24,** 1080–1093
72. Hulce, J. J., Cognetta, A. B., Niphakis, M. J., Tully, S. E., and Cravatt, B. F. (2013) Proteome-wide mapping of cholesterol-interacting proteins in mammalian cells. *Nat. Methods* **10,** 259–264
73. Harel, M., Aharoni, A., Gaidukov, L., Brumshtein, B., Khersonsky, O., Meged, R., Dvir, H., Ravelli, R. B., McCarthy, A., Toker, L., Silman, I., Sussman, J. L., and Tawfik, D. S. (2004) Structure and evolution of the serum paraoxonase family of detoxifying and anti-atherosclerotic enzymes. *Nat. Struct. Mol. Biol.* **11,** 412–419
74. Noto, H., Hashimoto, Y., Satoh, H., Hara, M., Iso-o, N., Togo, M., Kimura, S., and Tsukamoto, K. (2001) Exclusive association of paraoxonase 1 with high density lipoprotein particles in apolipoprotein A-I deficiency. *Biochem. Biophys. Res. Commun.* **289,** 395–401
75. Josse, D., Ebel, C., Stroebel, D., Fontaine, A., Borges, F., Echalier, A., Baud, D., Renault, F., Le Maire, M., Chabrieres, E., and Masson, P. (2002) Oligomeric states of the detergent-solubilized human serum paraoxonase (PON1). *J. Biol. Chem.* **277,** 33386–33397
76. Kuo, C. L., and La Du, B. N. (1995) Comparison of purified human and rabbit serum paraoxonases. *Drug Metab. Dispos.* **23,** 935–944
77. Gaidukov, L., and Tawfik, D. S. (2005) High affinity, stability, and lactonase activity of serum paraoxonase PON1 anchored on HDL with ApoA-I. *Biochemistry* **44,** 11843–11854
78. Wu, Z., Gogonea, V., Lee, X., Wagner, M. A., Li, X. M., Huang, Y., Undurti, A., May, R. P., Haertlein, M., Moulin, M., Gutsche, I., Zaccai, G., Didonato, J. A., and Hazen, S. L. (2009) Double superhelix model of high density lipoprotein. *J. Biol. Chem.* **284,** 36605–36619
79. Aviram, M., Hardak, E., Vaya, J., Mahmood, S., Milo, S., Hoffman, A., Billicke, S., Draganov, D., and Rosenblat, M. (2000) Human serum paraoxonases (PON1) Q and R selectively decrease lipid peroxides in human coronary and carotid atherosclerotic lesions: PON1 esterase and peroxidase-like activities. *Circulation* **101,** 2510–2517
80. Stevens, R. C., Suzuki, S. M., Cole, T. B., Park, S. S., Richter, R. J., and Furlong, C. E. (2008) Engineered recombinant human paraoxonase 1 (rHuPON1) purified from Escherichia coli protects against organophosphate poisoning. *Proc. Natl. Acad. Sci. U.S.A.* **105,** 12780–12784
81. Gaidukov, L., Bar, D., Yacobson, S., Naftali, E., Kaufman, O., Tabakman, R., Tawfik, D. S., and Levy-Nissenbaum, E. (2009) *In vivo* administration of BL-3050: highly stable engineered PON1-HDL complexes. *BMC Clin. Pharmacol.* **9,** 18
82. Rochu, D., Chabrière, E., and Masson, P. (2007) Human paraoxonase: a promising approach for pre-treatment and therapy of organophosphorus poisoning. *Toxicology* **233,** 47–59
83. Valiyaveettil, M., Alamneh, Y. A., Doctor, B. P., and Nambiar, M. P. (2012) Crossroads in the evaluation of paraoxonase 1 for protection against nerve agent and organophosphate toxicity. *Toxicol. Lett.* **210,** 87–94
84. Zhang, R., Brennan, M. L., Shen, Z., MacPherson, J. C., Schmitt, D., Molenda, C. E., and Hazen, S. L. (2002) Myeloperoxidase functions as a major enzymatic catalyst for initiation of lipid peroxidation at sites of inflammation. *J. Biol. Chem.* **277,** 46116–46122
85. Podrez, E. A., Febbraio, M., Sheibani, N., Schmitt, D., Silverstein, R. L., Hajjar, D. P., Cohen, P. A., Frazier, W. A., Hoff, H. F., and Hazen, S. L. (2000) Macrophage scavenger receptor CD36 is the major receptor for LDL modified by monocyte-generated reactive nitrogen species. *J. Clin. Invest.* **105,** 1095–1108
86. Brennan, M. L., Wu, W., Fu, X., Shen, Z., Song, W., Frost, H., Vadseth, C., Narine, L., Lenkiewicz, E., Borchers, M. T., Lusis, A. J., Lee, J. J., Lee, N. A., Abu-Soud, H. M., Ischiropoulos, H., and Hazen, S. L. (2002) A tale of two controversies: defining both the role of peroxidases in nitrotyrosine formation in vivo using eosinophil peroxidase and myeloperoxidase-deficient mice, and the nature of peroxidase-generated reactive nitrogen species. *J. Biol. Chem.* **277,** 17415–17427
87. Wang, Z., Nicholls, S. J., Rodriguez, E. R., Kummu, O., Hörkkö, S., Barnard, J., Reynolds, W. F., Topol, E. J., DiDonato, J. A., and Hazen, S. L. (2007) Protein carbamylation links inflammation, smoking, uremia and atherogenesis. *Nat. Med.* **13,** 1176–1184
88. Khersonsky, O., and Tawfik, D. S. (2006) The histidine 115-histidine 134 dyad mediates the lactonase activity of mammalian serum paraoxonases. *J. Biol. Chem.* **281,** 7649–7656
89. Rosenblat, M., Gaidukov, L., Khersonsky, O., Vaya, J., Oren, R., Tawfik, D. S., and Aviram, M. (2006) The catalytic histidine dyad of high density lipoprotein-associated serum paraoxonase-1 (PON1) is essential for PON1-mediated inhibition of low density lipoprotein oxidation and stimulation of macrophage cholesterol efflux. *J. Biol. Chem.* **281,** 7657–7665

Identification of Critical Paraoxonase 1 Residues Involved in High Density Lipoprotein Interaction

Xiaodong Gu, Ying Huang, Bruce S. Levison, Gary Gerstenecker, Anthony J. DiDonato, Leah B. Hazen, Joonsue Lee, Valentin Gogonea, Joseph A. DiDonato and Stanley L. Hazen

J. Biol. Chem. 2016, 291:1890-1904.
doi: 10.1074/jbc.M115.678334 originally published online November 13, 2015
